TRIM27 is an autophagy substrate facilitating mitochondria clustering and mitophagy via phosphorylated TBK1

Juncal Garcia-Garcia[1], Anne Kristin McLaren Berge[1], Katrine Stange Overå[1], Kenneth Bowitz Larsen[1], Zambarlal Bhujabal[1], Andreas Brech[2], Yakubu Princely Abudu[1], Trond Lamark[1], Terje Johansen[1] (iD) and Eva Sjøttem[1] (iD)

1 Department of Medical Biology, Autophagy Research Group, University of Tromsø –The Arctic University of Norway, Norway
2 Department of Molecular Cell Biology, Institute for Cancer Research, Oslo University Hospital, Norway

Tripartite motif-containing protein 27 (TRIM27/also called RFP) is a multifunctional ubiquitin E3 ligase involved in numerous cellular functions, such as proliferation, apoptosis, regulation of the NF-kB pathway, endosomal recycling and the innate immune response. TRIM27 interacts directly with TANK-binding kinase 1 (TBK1) and regulates its stability. TBK1 in complex with autophagy receptors is recruited to ubiquitin chains assembled on the mitochondrial outer membrane promoting mitophagy. Here, we identify TRIM27 as an autophagy substrate, depending on ATG7, ATG9 and autophagy receptors for its lysosomal degradation. We show that TRIM27 forms ubiquitylated cytoplasmic bodies that co-localize with autophagy receptors. Surprisingly, we observed that induced expression of EGFP-TRIM27 in HEK293 FlpIn TRIM27 knockout cells mediates mitochondrial clustering. TRIM27 interacts with autophagy receptor SQSTM1/p62, and the TRIM27-mediated mitochondrial clustering is facilitated by SQSTM/p62. We show that phosphorylated TBK1 is recruited to the clustered mitochondria. Moreover, induced mitophagy activity is reduced in HEK293 FlpIn TRIM27 knockout cells, while re-introduction of EGFP-TRIM27 completely restores the mitophagy activity. Inhibition of TBK1 reduces mitophagy in HEK293 FlpIn cells and in the reconstituted EGFP-TRIM27-expressing cells, but not in HEK293 FlpIn TRIM27 knockout cells. Altogether, these data reveal novel roles for TRIM27 in mitophagy, facilitating mitochondrial clustering via SQSTM1/p62 and mitophagy via stabilization of phosphorylated TBK1 on mitochondria.

Abbreviations

AMPK, adenosine 5′-monophosphate-activated protein kinase; ATG, autophagy-related protein; CC, coiled-coil; CLEM, correlative light and electron microscopy; EGFP, enhanced green fluorescent protein; ER, endoplasmatic reticulum; FKBP8, FK506-binding protein 8; GST, gluthattathione-S-transferase; HEK293, human embryonic kidney 293 cells; KO, knock out; LAMP1, lysosome-associated membrane glycoprotein 1; LC3, mmicrotubule-associated proteins 1A/1B light chain 3; LIR, LC3-interacting region; NBR1, next to BRCA1 gene 1 protein; NDP52, nuclear domain 10 protein 52; OMM, outer mitochondrial membrane; OMP25, 25 kDa outer-membrane immunogenic protein; PINK1, PTEN-induced putative kinase 1; RFP, Ret finger protein; SQSTM1/p62, sequestosome 1; TBK1, TANK-binding kinase 1; TM, transmembrane; TNF-α, tumour necrosis factor alpha; TOM20, translocase of outer mitochondrial membrane 20; TRIM, tripartite motif-containing protein; ULK1, unc-51-like kinase; USP7, ubiquitin-specific peptidase 7; WIPI2, WD repeat domain phosphoinositide-interacting protein 2; WT, wild-type.

Introduction

Ubiquitylation is a reversible posttranslational modification with high specificity, which regulates multiple cellular processes such as organelle quality control, protein degradation, signal transduction, cell-cycle progression, receptor trafficking and endocytosis and the immune response [1–3]. Ubiquitin E3 ligases mediate the transfer of ubiquitin to substrate proteins determining their fate. Tripartite motif family proteins (TRIMs) constitute a large family of ubiquitin E3 ligases involved in several cellular processes such as intracellular signalling, innate immunity, transcription, autophagy and carcinogenesis [4]. TRIM proteins are characterized by their N-terminal RBCC domain consisting of a RING-finger domain (R), one or two B-boxes (B1/B2) and a coiled-coil (CC) domain. In addition, most TRIMs exhibit domains at the C terminus, which gives them specificity for their target proteins [5]. TRIM proteins are implicated in several steps of the autophagy process, ranging from regulation of upstream signalling pathways to autophagosome formation and autophagy receptor activity [6]. TRIMs are reported to act as platforms for early autophagic structures through the assembly of the autophagy proteins ULK1 and Beclin1 [7–10]. They can act as autophagy receptors, such as TRIM5α and TRIM23, by recognizing and targeting viral proteins for autophagic degradation [11,12], or they regulate autophagy through their activation of the autophagy receptor SQSTM1/p62 [12–14].

TRIM27 was originally described as a fusion protein with the tyrosine kinase domain of the c-RET proto-oncogene [15]. It is ubiquitously expressed and localized both in the cytoplasm and in the nucleus of the cells, depending on the cell type [16]. TRIM27 is a multifunctional protein involved in the regulation of several cellular processes such as innate immunity, apoptosis, cell growth, proliferation and endosomal recycling [17–21]. It has several roles in host defence against pathogens, acting as a host restriction factor during mycobacterial infection, enhancing immune-inflammatory response and cell apoptosis [22]. In addition, TRIM27 has been identified as a degradation target of Herpes Simplex Virus 1 ICP0 [23], and together with the ubiquitin-specific protease, USP7 negatively modulates antiviral type I interferon signalling via regulation of TANK-binding kinase 1 (TBK1) stability [24]. The TRIM27-USP7 dimer is shown to form a complex with receptor-interacting protein 1 (RIP1), promoting its de-ubiquitylation resulting in TNF-α-induced apoptosis [25]. Moreover, TRIM27 and USP7 play a role in endosomal recycling when they are in complex with MAGE-L2. This complex regulates the activity of WASH/retromer-mediated endosomal recycling through ubiquitylation events [26].

Mitochondrial quality control is crucial to preserve cellular respiration and respond to mitochondrial damage. The mitochondrial quality control pathway includes a comprehensive quality assurance apparatus, including the selective clearance of damaged or dysfunctional mitochondria by lysosomes via autophagy, termed mitophagy (recently reviewed in [27]). Ubiquitylation is an important signal for the activation of mitophagy, and targeting the outer mitochondrial membrane (OMM) by short ubiquitin chains is sufficient to induce mitophagy [28]. The best studied mitophagy pathway is the PTEN-induced putative kinase 1 (PINK1)/PARKIN pathway. Upon loss of mitochondrial membrane potential, PINK1 is stabilized and activated at the OMM, facilitating ubiquitin phosphorylation at Serine 65 and recruitment of the ubiquitin E3 ligase PARKIN. Parkin is phosphorylated at an equivalent Ser65 residue located within its N-terminal ubiquitin-like domain, resulting in activation [29–32]. Ubiquitylation of OMM proteins provides a docking site for the sequestosome-like autophagy receptors such as SQSTM1/p62 [33], thereby bridging the ubiquitylated mitochondria to the autophagosome. TBK1 plays an important signalling role in this process, activating the autophagy receptors by phosphorylation events that increase their ability to bind ubiquitin [34–37]. However, also PARKIN-independent mitophagy pathways are identified. These pathways involve molecules localized on the mitochondria, such as FKBP8, FUNDC1, BNIP3, BCL2-L-13, BNIP3L/NIX and cardiolipin, acting as mitophagy receptors tethering the mitochondria to the autophagosome [38]. Additionally, the adenosine 5′-monophosphate (AMP)-activated protein kinase (AMPK) is emerging as a key player in mitophagy, facilitating mitochondrial fission and autophagosomal engulfment via TBK1 activation [39].

In a previous study, we identified TRIM27 as a potential substrate for autophagic degradation [13]. Since TRIM27 is recognized to play a role in the endo-lysosomal system, the objective of this study was to elucidate whether TRIM27 has a role in autophagy. We show that TRIM27 is a cargo for the sequestosome-like receptors, associating with late autophagy structures. To characterize the impact of TRIM27 on the autophagy process, we established a HEK293 FlpIn TRIM27 KO cell line with inducible expression of EGFP-TRIM27. By correlative electron microscopy and fluorescence confocal imaging, we observed a strong tendency of mitochondrial clustering in the cells expressing EGFP-TRIM27. We show that

pTBK1 and SQSTM1/p62 are recruited to these mito-chondria clusters, while inhibition of TBK1 activity alleviates these clusters. We find that TRIM27 co-localizes with SQSTM1/p62 and pTBK1 in cytoplas-mic structures that are closely associated with the mitochondria. Finally, we show that knock-down of TRIM27 in the HEK293 FlpIn cells impairs FKBP8/LC3A induced mitophagy, while re-introduction of EGFP-TRIM27 strongly promotes mitophagy in a pTBK1-dependent pathway.

Results

Autophagic degradation of TRIM27 is dependent on ATG7 and autophagy receptors

In a qualitative screen performed in HeLa cells using the double-tag mCherry-EYFP fused to 22 various members of the TRIM family of ubiquitin E3 ligases, we identified TRIM27 as a potential target for autop-hagic degradation [13]. We observed RedOnly puncta in the mCherry-EYFP-TRIM27-expressing cells (Fig. 1A), with an increased induction of RedOnly puncta upon starvation (Fig. 1B). Macroautophagy can be divided into conventional ATG7-dependent autophagy and ATG7-independent alternative autop-hagy [40,41]. To pinpoint the autophagy pathway implicated in TRIM27 degradation, the mCherry-EYFP-TRIM27 expression plasmid was transfected into a HeLa ATG7 KO cell line. We were not able to observe any RedOnly dots in the ATG7 KO cells 1-day post-transfection (Fig. 1A,B), indicating that autophagic degradation of TRIM27 is dependent on the conventional autophagy pathway.

To investigate whether TRIM27, such as TRIM5α, has the ability to act as an autophagy receptor and hence can be degraded by autophagy independent of other receptors, the mCherry-EYFP-TRIM27 double-tag assay was applied on a HeLa cell line knocked out for the five autophagy receptors SQSTM1/p62, NBR1, NDP52/Calcoco2, Optineurin and Tax1BP1 (HeLa pentaKO) [33]. No RedOnly dots of mCherry-EYFP-TRIM27 could be observed neither under normal nor starved conditions (Fig. 1A,B). This indicates that autophagic degradation of TRIM27 is dependent on the sequestosome-like autophagy receptors, and for this reason, TRIM27 might not act as an autophagy receptor itself. To verify this further, we applied the mCherry-EYFP-TRIM27 double-tag assay on the HeLa pentaKO cell line reconstituted with EGFP-SQSTM1/p62 (Fig. 1A,B) [13]. Expression of EGFP-SQSTM1/p62 in the HeLa pentaKO cell line was suffi-cient to direct lysosomal degradation of mCherry-

EYFP-TRIM27, but not to the same extent as the HeLa wild-type cells (Fig. 1B). This suggests that TRIM27 can be degraded by selective autophagy and that it is dependent on the sequestosome-like receptors for being degraded by a lysosomal pathway. Hence, TRIM27 does not act as an autophagy receptor itself.

In order to determine whether endogenous TRIM27 is degraded by autophagy, we analysed the TRIM27 protein levels in HeLa ATG9 KO cells. ATG9 vesicles are required for nucleation of the autophagic isolation membrane, and therefore ablation of ATG9 will block the autophagy process [42]. Notably, TRIM27 seems to be stabilized and modified in the ATG9 KOs cells. The stronger TRIM27 band with reduced mobility suggests that inhibition of autophagy by ATG9 KO has impact on both TRIM27 modification and expres-sion level (Fig. 1C,D). The autophagy receptors SQSTM1/p62 and NBR1 also display stronger bands with lower mobility in extracts from HeLa ATG9 KO cells than normal HeLa cells (Fig. 1C), supporting the link between the sequestosome-like autophagy recep-tors and TRIM27 autophagic degradation.

TRIM27 forms cytoplasmic bodies that co-localizes with autophagy receptors

To further address the association of TRIM27 with selective autophagy, our next step was to analyse whether TRIM27 co-localizes with autophagy struc-tures in cells. Since we were not able to find a TRIM27 antibody that worked well in immunofluores-cence assays, we established a HEK293 FlpIn TRIM27 KO cell line by CRISPR/Cas9 [43] and reconstituted this KO cell line with tetracycline-inducible expres-sion of EGFP-TRIM27 (Fig. 2A–D). EGFP-TRIM27 formed several cytoplasmic bodies in addition to a few nuclear puncta, and in some cells, EGFP-TRIM27 formed larger irregular structures (Fig. 2E). This is in line with the reported localization of endogenous TRIM27 in HEK293 cells [44] and NIH3T3 cells [45], indicating that induced EGFP-TRIM27 is representa-tive for endogenous TRIM27. We further analysed the proliferation and migration potential of the HEK293 FlpIn TRIM27 KO cells and the reconstituted TRIM27 KO cell lines (Fig. 2F). The HEK293 FlpIn TRIM27 KO cell line displays an enhanced prolifera-tion rate compared with the HEK293 FlpIn TRIM27 KO cell line reconstituted with EGFP-TRIM27 (Fig. 2F, left graph). This suggests that TRIM27 expression may inhibit cell proliferation in HEK293 FlpIn cells, which may be due to the role of TRIM27 in promoting TNF-α-induced apoptosis [25]. Con-versely, the migration rate of the TRIM27 KO cells
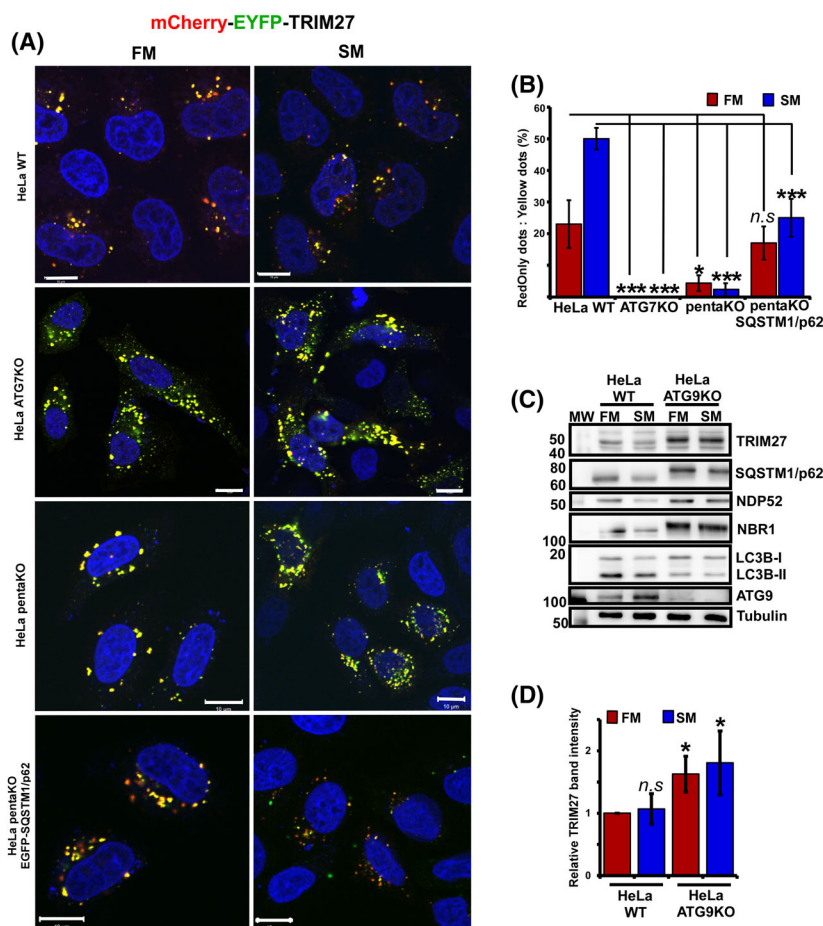
Fig. 1. Autophagic degradation of TRIM27 is dependent on ATG7, ATG9 and the Sequestosome-like receptors. (A) Normal HeLa cells and HeLa cells that were genetically knocked out for ATG7, the 5 autophagy receptors SQSTM1/p62, NBR1, NDP52, optineurin and Tax1BP1 (pentaKO) or pentaKO cells with reintroduced EGFP-SQSTM1/p62 were transfected with mCherry-EYFP-TRIM27 expression plasmids. One-day post-transfection, the cells were treated with HBSS for 2 h (SM) or incubated in full medium (FM), before all cells were fixated, stained with DAPI and imaged using a LSM780 confocal microscope (ZEISS). Scale bar: 10 μm. (B) The graphs represent the amount of yellow dots and RedOnly dots in the mCherry-EYFP-TRIM27 transfected cells shown with representative images in (A). The graphs show the average values obtained in three independent experiments with s. (D). Normal (FM) and starved (HBSS 2 h; SM) conditions. ***: $P < 0.0005$ using Student's t-test *: $P < 0.05$ using Student's t-test; n.s.: $P > 0.05$ using Student's t-test. (C) Western blot analysis of endogenous TRIM27, the autophagy receptor SQSTM1/p62, NDP52, and NBR1, and LC3B in HeLa WT and HeLa ATG9 KO cells in normal medium (FM) or treated with HBSS (SM) for 4 h. (D) Quantification of the intensity of TRIM27 bands in western blot analysis as displayed in (C). The graph represents the average of three independent experiments with SD *: $P < 0.05$; n.s.: $P > 0.05$ (Student's t-test).

was reduced compared with the HEK293 FlpIn cells, while re-introduction of EGFP-TRIM27 restored the migration rate (Fig. 2F, right graph). Thus, in HEK293 FlpIn cells, TRIM27 seems to facilitate cell migration but not cell proliferation. This is in line with previous studies showing that TRIM27 facilitates cell migration and invasion [46] and may have a role in epithelial-to-mesenchymal transition in cancer cells.

To analyse whether the cytoplasmic EGFP-TRIM27 bodies are associated with autophagy structures, the HEK293 FlpIn TRIM27 KO cells induced to express

EGFP-TRIM27 were immunostained with antibodies against various autophagy marker proteins. First, we observed that the EGFP-TRIM27 bodies did not co-localize with GM130 (Golgi marker) or calreticulin (ER marker), suggesting that TRIM27 is not a Golgi- or ER-associated protein (Fig. 3). This is in line with a previous paper on TRIM27 subcellular localization, where they reported no Golgi- or ER-targeting signals in TRIM27 [45]. However, EGFP-TRIM27 co-localized in several cytoplasmic dots with the autophagy receptors SQSTM1/p62 and NBR1 (Fig. 4A).

(A) TRIM27 Exon1 (Guide sequence):

```
atggcctccgggagtgtggccgagtgcctgcagcaggagaccacctgccccgtgtgcctgcagtacttcgcagagcccatgatgctcgactgcg
gccataacatctgttgcgcgtgcctcgcccgctgctggggcacggcagagactaacgtgtcgtgcccgcagtgccgggagaccttccgcagag
gcacatgcgggcccaaccggcacctggccaacgtgacccaactggtaaagcagctgcgca
```

A1 (140 nt deletion + 9 nt insertion):

```
atggcctccgggagtgtggccgagtgcctgcagcaggagaccacctgccccgtgtgcctgcagtacttcgcagagcccat.............
..........................aatgctcga.............................................
..............................acgtgacccaactggtaaagcagctgcgca
```

A2 (133 nt deletion + 2 nt insertion):

```
Atggcctccgggagtgtggccgagtgcctgcagcaggagaccacctgccccgtgtgcctgcagtacttcgcagagcccatgatgctcgactg..
..................................aa.............................................
..............................tgacccaactggtaaagcagctgcgca
```
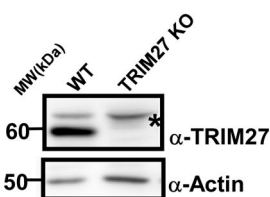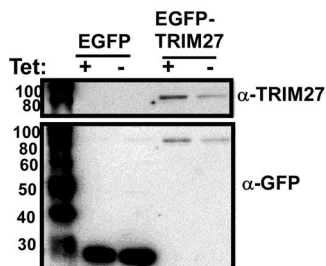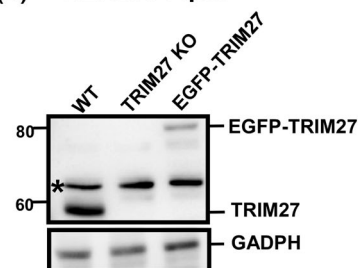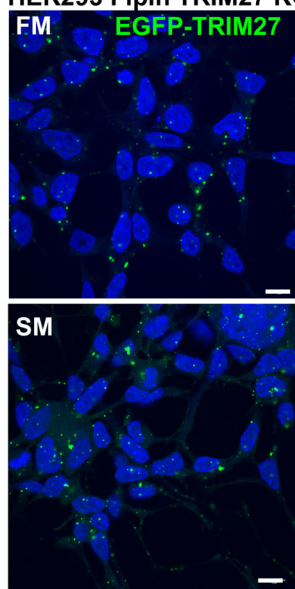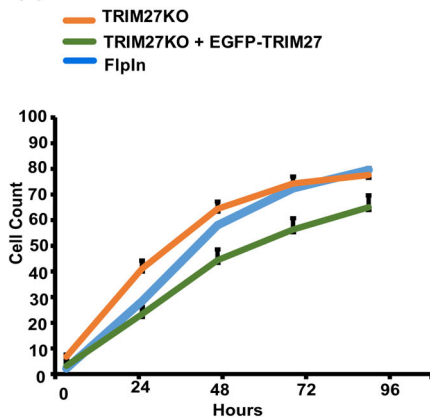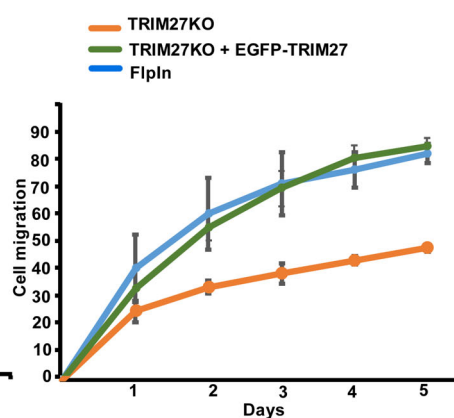

Fig. 2. TRIM27 localizes to cytoplasmic bodies and facilitates cell migration of HEK 293T FlpIn cells. (A) DNA sequences encompassing the target sequence employed in the CRISPR/Cas9 mediated strategy generation TRIM27 KO cell line. The lower part shows the DNA sequences of the PCR products obtained from the genomic loci targeted by CRISPR/Cas9. (B) Western blot analysis of HEK293 FlpIn cells and the TRIM27 KO cells, showing KO of TRIM27. The * indicates an unspecific band detected by the TRIM27 antibody. (C) Western blot analysis of HEK293 FlpIn TRIM27 KO cells reconstituted with tetracycline-inducible expression of EGFP or EGFP-TRIM27. Expression of EGFP and EGFP was detected by an anti-GFP antibody. Tetracycline (0.1 µg·µL^{-1}) was added where indicated above the blot. (D) Western blot analysis comparing expression of endogenous TRIM27 in the HEK293 FlpIn cells and tetracycline (0.1 µg·µL^{-1}) induced expression of EGFP-TRIM27 in the reconstituted HEK293 FlpIn TRIM27 KO cell lines. The proteins were detected using an anti-TRIM27 antibody. The * indicates an unspecific band detected by the TRIM27 antibody. (E) Representative images of EGFP-TRIM27 expressed in the reconstituted HEK293 FlpIn TRIM27 KO cell lines, upon normal (FM) and starved (SM) (HBSS 2 h) conditions. Images were obtained using a ZEISS780 confocal laser scanning microscope. Scale bar 10 µm. (F) Proliferation (left graph) and migration (right graph) curves of HEK293 FlpIn, HEK293 FlpIn TRIM27 KO and HEK293 FlpIn TRIM27 KO reconstituted with EGFP-TRIM27. The graphs were obtained using the IncuCyte® S3 Live-Cell Analysis System (Sartorius). Error bars indicate SD of independent experiments ($n = 3$ for proliferation, $n = 2$ for migration).
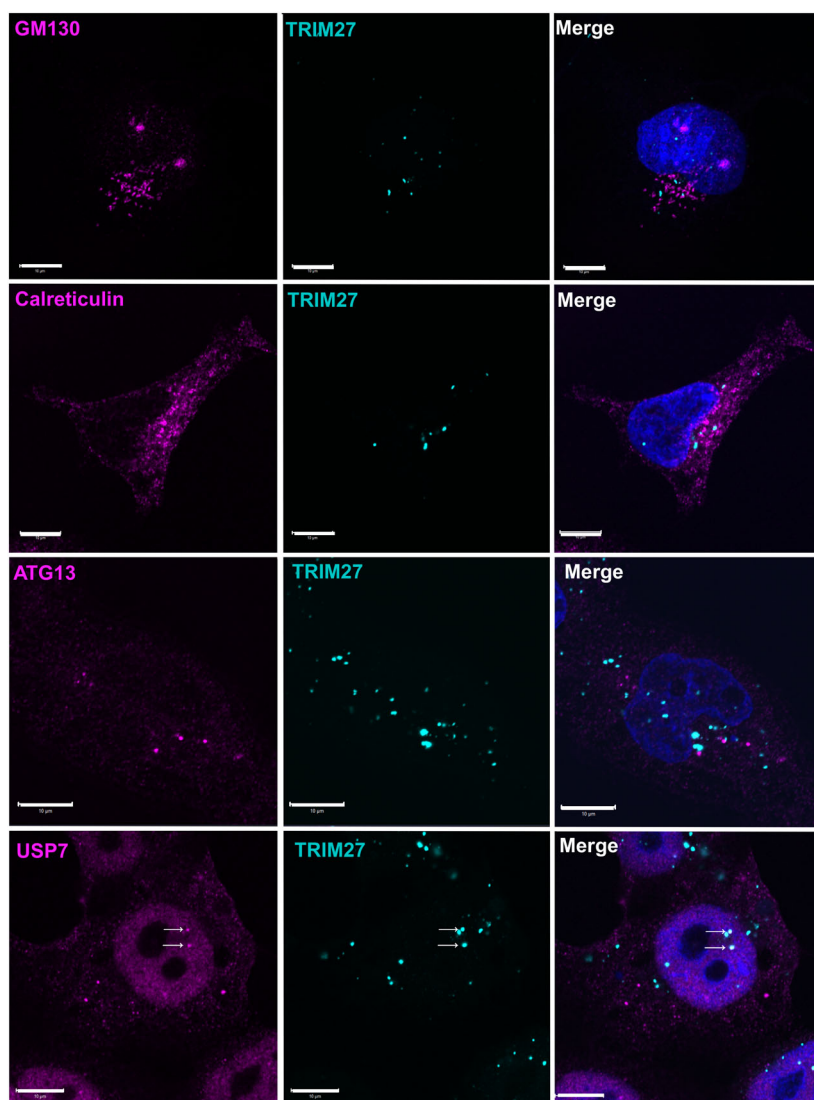
Fig. 3. Representative images of HEK293 FlpIn TRIM27 KO cells reconstituted with EGFP-TRIM27 fixed and stained with antibodies for GM130, calreticulin, USP7 or ATG13 as indicated. Images were obtained using a ZEISS780 confocal laser scanning microscope. Scale bar 10 μm.

Moreover, the autophagosome marker protein LC3B co-localized with EGFP-TRIM27 in some dots, while structures stained by the late autophagosome/lysosome marker protein LAMP1 associated closely with EGFP-TRIM27 (Fig. 4A). These data support that TRIM27 can be degraded by selective autophagy. However, EGFP-TRIM27 did not co-localize with early autophagy structures, such as WIPI2 (Fig. 4A) or ATG13 (Fig. 3). In order to verify the EGFP-TRIM27 localization pattern, we stained the HEK293 FlpIn TRIM27 KO EGFP-TRIM27 cells with antibodies towards USP7 and ubiquitin. We applied the FK2 antibody that recognizes both mono and polyubiquitin (FK2). It is well recognized that TRIM27 forms a complex with USP7 that is implicated in the regulation of tumour necrosis factor alpha-induced apoptosis [25]. TRIM27 also forms a complex with USP7 and

MAGE-L2, and this complex regulates the protein levels of WASHC1 that is involved in endosomal sorting and vesicles trafficking [24]. In accordance with this, we see that USP7 is present in certain EGFP-TRIM27 dots (Fig. 3). Moreover, most of the cytoplasmic EGFP-TRIM27 bodies are recognized by the ubiquitin FK2 antibody (Fig. 4B), revealing that the cytoplasmic TRIM27 bodies are highly ubiquitylated and/or strongly associated by ubiquitin molecules. This is in line with the work by Zaman et al., 2013, suggesting that autoubiquitylation of TRIM27 is required for its cytoplasmic localization. Importantly, some ubiquitylated EGFP-TRIM27 bodies were detected inside ring-like structures that stained positive for the antibody towards LAMP1, further supporting that TRIM27 is an autophagy substrate (Fig. 4B). Thus, TRIM27 forms ubiquitylated bodies in the cytoplasm
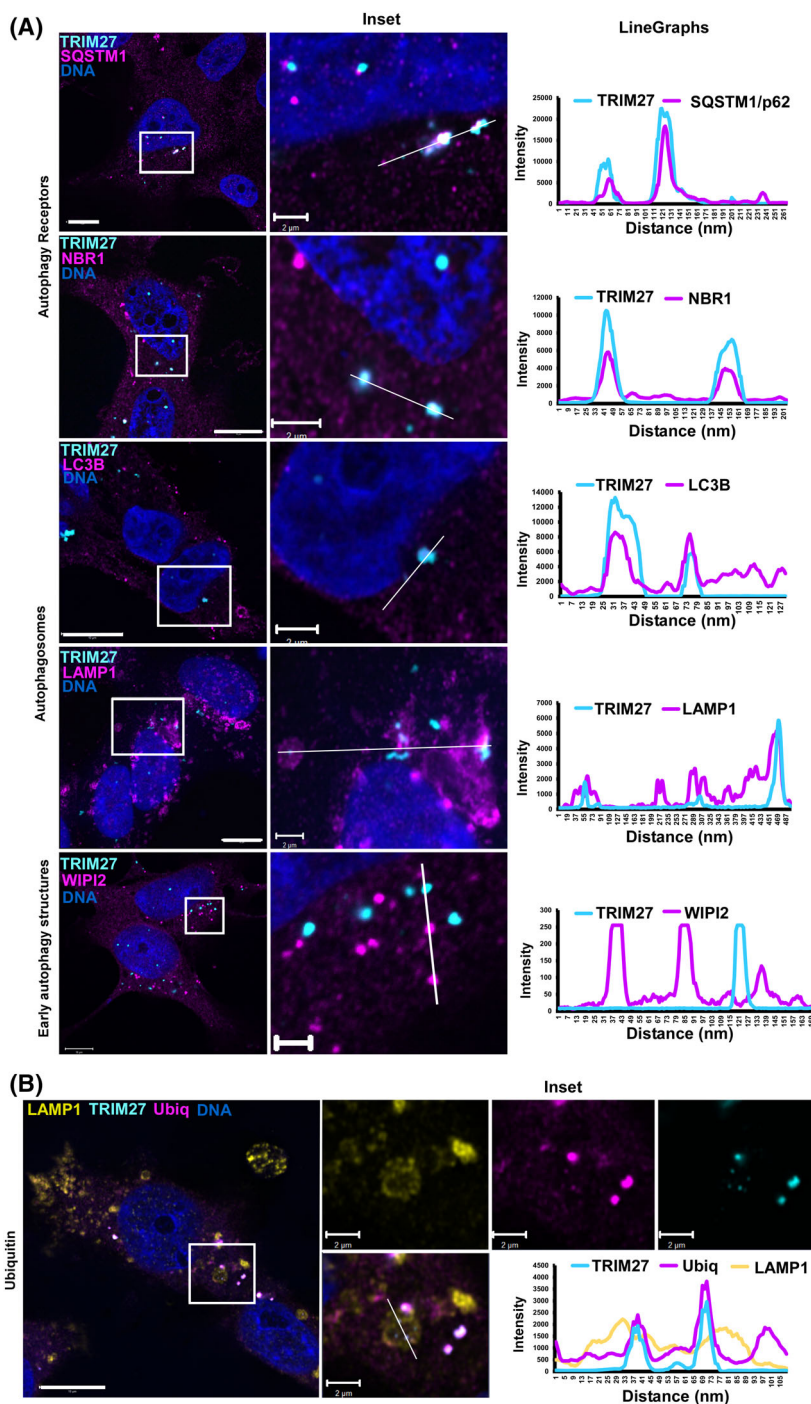
Fig. 4. TRIM27 co-localizes with autophagy receptors. (A) Representative images of HEK293 FlpIn TRIM27 KO EGFP-TRIM27 cells fixed and stained with antibodies for SQSTM1/p62, NBR1, LC3B, LAMP1 and WIPI2. Images were obtained using a LSM880 with Airyscan (ZEISS), and co-localization monitored using the ZEN LITE software. Intensity profiles along the indicated lines in the insets are shown to the right. Scale bars: 10 μm, insets: 2 μm. (B) Representative images of HEK293 FlpIn TRIM27 KO EGFP-TRIM27 cells fixed and stained with antibodies for LAMP1 and ubiquitin (FK2 antibody). Images were obtained as described in (A).

that co-localize with sequestosome-like autophagy receptors.

TRIM27 induces mitochondrial clustering

In an attempt to characterize the ultrastructure of the cytoplasmic EGFP-TRIM27 bodies, we performed CLEM (Correlative Light and Electron Microscopy) analyses of the HEK293 FlpIn TRIM27 KO EGFP-TRIM27 cells. Surprisingly, we observed that the mitochondria displayed an abnormal morphology and were clustered in perinuclear regions in the cells that expressed EGFP-TRIM27 (Fig. 5A). To determine whether mitochondrial clustering was a general
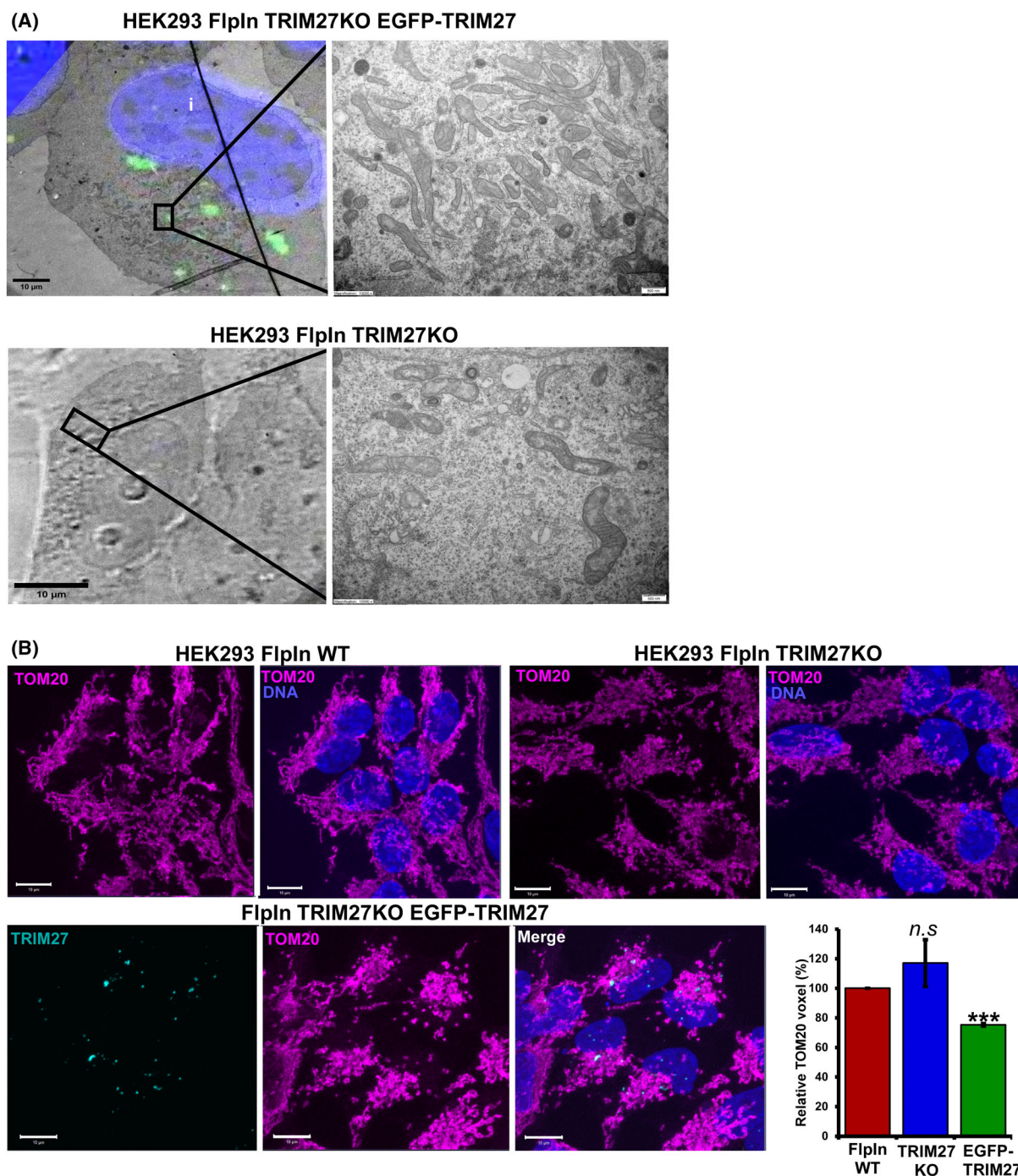
Fig. 5. TRIM27 expression promotes mitochondrial clustering. (A) HEK293 FlpIn TRIM27 KO cells induced to express EGFP-TRIM27 (upper panels) and HEK293 FlpIn TRIM27 KO cells (lower panels) were fixed 1-day postinduction and imaged by fluorescence confocal microscopy to localize cells containing cytoplasmic EGFP-TRIM27 bodies. The cells were subsequently processed for transmission electron microscopy. Following ultramicrotomy, cells of interest were relocalized within sections and imaged at both intermediate and high magnifications to analyse the surrounding cellular environment and ultrastructural details. Scale bars: 500 nm (B) representative images of HEK293 FlpIn (upper left panels), HEK293 FlpIn TRIM27 KO (upper right panels) and HEK293 FlpIn TRIM27 KO EGFP-TRIM27 (lower panels) cells fixed and stained with antibodies for TOM20. Images were obtained using a LSM 780 (ZEISS) fluorescence confocal microscope. The graphs represent average with SD of relative mitochondria voxel quantified using VOLOCITY (Perkin Elmer) of z-stack images of > 100 cells per condition per experiment, from three independent experiments. ***: $P < 0.0005$; n.s.: $P > 0.05$ (Student's t-test). Scale bars: 10 μm.

phenotype in cells expressing EGFP-TRIM27, we immunostained the mitochondria in the HEK293 FlpIn cells, the HEK293 FlpIn TRIM27 KO cells and the TRIM27 KO cells reconstituted with EGFP-TRIM27 by antibodies against the outer membrane mitochondrial protein TOM20 (Fig. 5B). Quantification of the mitochondria voxel within each of these cell lines displayed a significant reduction of the mitochondria voxel in the TRIM27 KO cells that were reconstituted with inducible expression of EGFP-TRIM27 (Fig. 5B). The images reveal that many EGFP-TRIM27 bodies are localized close to the mitochondria, and some are partially overlapping with the mitochondria. A partial localization of TRIM27 with MitoTracker, a mitochondria-selective fluorescent label, was reported by Zaman et al., 2013. They reported that TRIM27 was localized in the mitoplast or tightly associated with the inner membrane, with the N-terminal region located on the outer mitochondria membrane. Together these findings suggest that TRIM27 is partially localized to mitochondria and can promote mitochondria clustering.

SQSTM1/p62 facilitates TRIM27-mediated mitochondrial clustering

Polyubiquitylations of OMM proteins are shown to recruit autophagy receptor SQSTM1/p62 to the mitochondria [47,48]. SQSTM1/p62 mediates clustering of dysfunctional mitochondria through polymerization via its PB1 domain [32,48]. SQSTM1/p62-mediated clustering of mitochondria is not important for PINK1/PARKIN-driven mitophagy. However, SQSTM1/p62 is reported to be essential for NLRP3 agonist-induced mitophagy [49] and mitophagy in leukaemia cells [50]. The localization SQSTM1/p62 in TRIM27 bodies raised the question whether SQSTM1/p62 was implicated in the TRIM27-mediated mitochondrial clustering. Confocal imaging of endogenous SQSTM1/p62 in the HEK293 FlpIn cells, the HEK293 FlpIn TRIM27KO cells and the HEK293 FlpIn TRIM27KO cells reconstituted with EGFP-TRIM27 revealed that SQSTM1/p62 was relocalized to larger structures in the EGFP-TRIM27-expressing cells (Fig. 6A). Around 68 ($\pm$9)% of the SQSTM1/p62 structures co-localized with EGFP-TRIM27, while 46 ($\pm$3)% of the EGFP-TRIM27 bodies stained for SQSTM1/p62. Hence, these two proteins have a tendency to localize in the same subcellular structures, but they also form cytoplasmic bodies independent of each other. Association between TRIM27 and SQSTM1/p62 in cells was verified by immunoprecipitation assays (Fig. 6B), while *in vitro* GST-pulldown

assays using GST-SQSTM/p62 expressed and purified from *Escherichia coli* and *in vitro* translated TRIM27 indicated that TRIM27 can interact directly with SQSTM1/p62 (Fig. 6C). Importantly, co-staining of the HEK293 FlpIn TRIM27 KO cells induced to express EGFP-TRIM27 with antibodies towards SQSTM1/p62 and the OMM protein TOM20 showed that SQSTM1/p62 bodies are localized on the clustered mitochondria (Fig. 6D). To investigate whether SQSTM1/p62 was implicated in the TRIM27-mediated mitochondrial clustering, EGFP-TRIM27 was ectopically expressed in HEK293 SQSTM1/p62 knockout cells [13]. Measurement of the mitochondria voxel in the HEK293 SQSTM1/p62 knockout cells and wild-type HEK293 cells, both with ectopically expressed EGFP-TRIM27, showed that ablation of SQSTM1/p62 alleviated the mitochondrial clustering induced by EGFP-TRIM27 (Fig. 6E). This indicates that SQSTM1/p62 is implicated in the mitochondrial clustering promoted by TRIM27.

TRIM27-mediated mitochondria clustering implicates TBK1 activity

Previous studies have shown that efficient recruitment of SQSTM1/p62 and other autophagy receptors to damaged mitochondria is dependent on TBK1 activation [36,51]. TBK1 is transiently recruited to polyubiquitylated mitochondria, and autophosphorylates locally [52]. Activated TBK1 phosphorylates SQSTM1/p62 at S403 located in the ubiquitin-binding domain [35]. SQSTM1/p62 phosphorylation at S403 is required for efficient binding of it to ubiquitylated substrates [35,53,54]. We thus raised the question whether TBK1 played a role in the TRIM27-mediated clustering of mitochondria. To answer this, we first analysed if active TBK1 was associated with the clustered mitochondria by fluorescence confocal imaging. Figure 7A shows that S172 phosphorylated TBK1 is strongly enriched on the clustered mitochondria. The intensity line graphs identify recruitment of pTBK1 to TRIM27 bodies, in addition to strong enrichment of pTBK1 on the clustered mitochondria. The localization of pTBK1 in TRIM27 bodies supports a previous report showing that TRIM27 and TBK1 interact directly via their coiled-coil regions [19]. The locally enrichment of pTBK1 in TRIM27 bodies may lead to its activation via autophosphorylation events [55]. Quantification of the amount of pTBK1 on mitochondria in the HEK293 FlpIn, HEK293 FlpIn TRIM27 KO and HEK293 FlpIn TRIM27 KO reconstituted with EGFP-TRIM27 verifies the enhanced localization of pTBK1 on the mitochondria in the EGFP-TRIM27
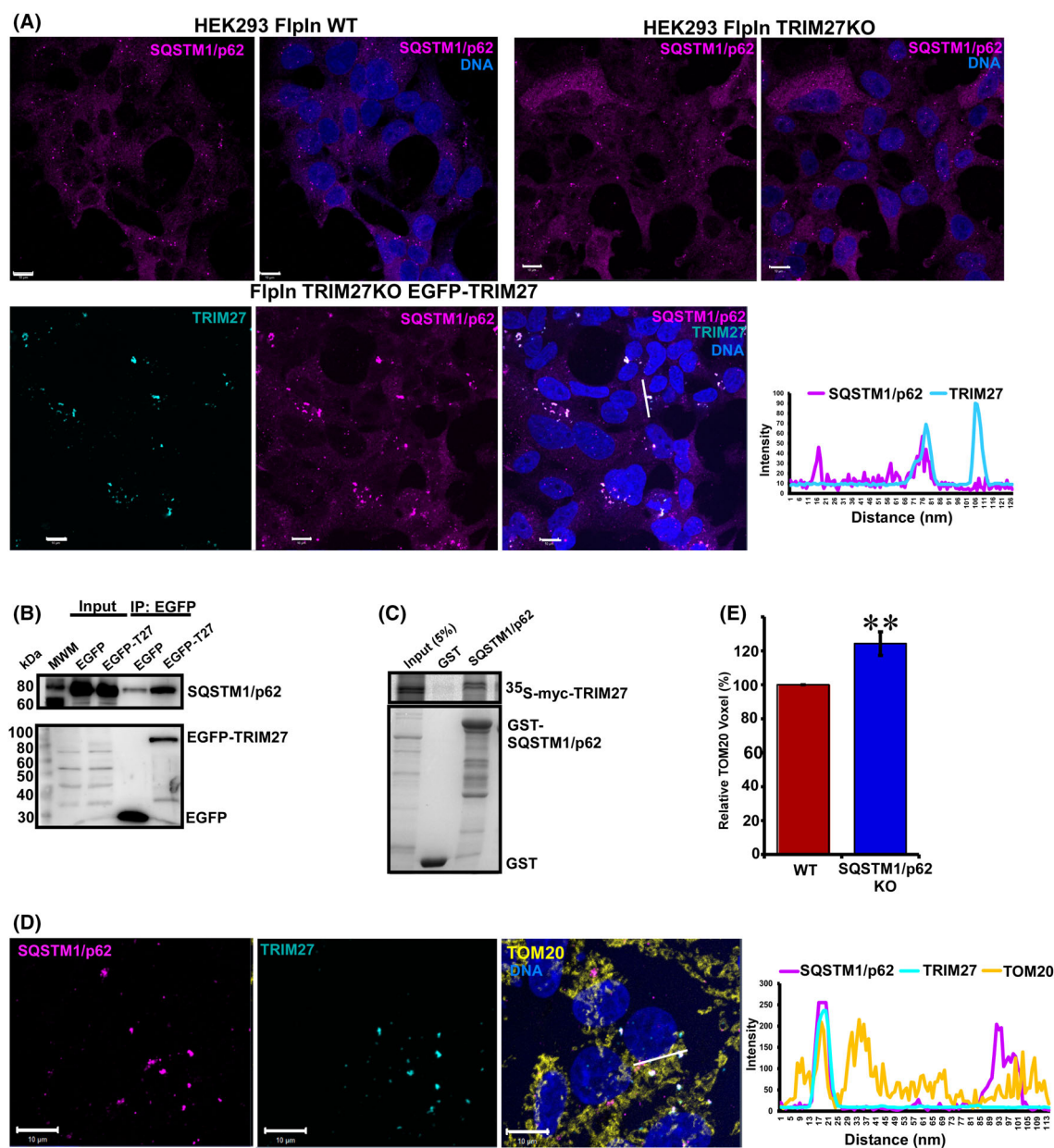
Fig. 6. TRIM27 interacts with SQSTM1/p62, and SQSTM1/p62 facilitates TRIM27-mediated mitochondria clustering. (A) Immunostaining of SQSTM1/p62 in HEK293 FlpIn (upper left panels), HEK293 FlpIn TRIM27 KO (upper right panels) and HEK293 FlpIn TRIM27 KO reconstituted with inducible expression of EGFP-TRIM27 (lower panels). Images were obtained using a LSM780 confocal laser scanning microscope (ZEISS), and the co-localization line plot to the right obtained using the ZEN LITE software (ZEISS). Scale bars: 10 μm. (B) Immunoprecipitated extracts from HEK293 FlpIn TRIM27 KO cells reconstituted with inducible expression (0.1 μg·μL^{-1} doxycycline, 20 h) of EGFP or EGFP-TRIM27 as indicated. EGFP and EGFP-TRIM27 were immunoprecipitated by a GFP-TRAP, and detected by western blot using an anti-GFP antibody (lower left panel). Co-precipitated SQSTM1/p62 was detected by an anti-SQSTM1/p62 antibody (upper left panel). (C) Representative GST-pulldown assay using ^{35}S-labelled myc-TRIM27 and recombinant GST and GST-SQSTM1/p62 proteins as indicated. The amount of TRIM27 bound to GST and GST-SQSTM1/p62 was detected by autoradiography. The assay was repeated with similar results. (D) Confocal images showing the localization of endogenous SQSTM1/p62, EGFP-TRIM27 and mitochondria (stained with an anti-TOM20 antibody) in the HEK293 FlpIn TRIM27KO cells with induced expression of EGFP-TRIM27 (0.1 μg·μL^{-1} doxycycline, 20 h). The co-localization line plot to the right was obtained using the ZEN LITE software (ZEISS). Scale bars: 10 μm. (E) Quantification of the amount of mitochondria (TOM20 intensity and volume) in HEK293 and HEK293 SQSTM1/p62 KO cell lines transiently expressing EGFP-TRIM27. Quantification of mitochondria voxel was performed on fixed cells 1-day post-transfection using VOLOCITY software (Perkin Elmer). The graphs represent the average of three independent experiments with SD, each experiment including > 80 cells per condition. **$P < 0.005$ (Student's t-test).
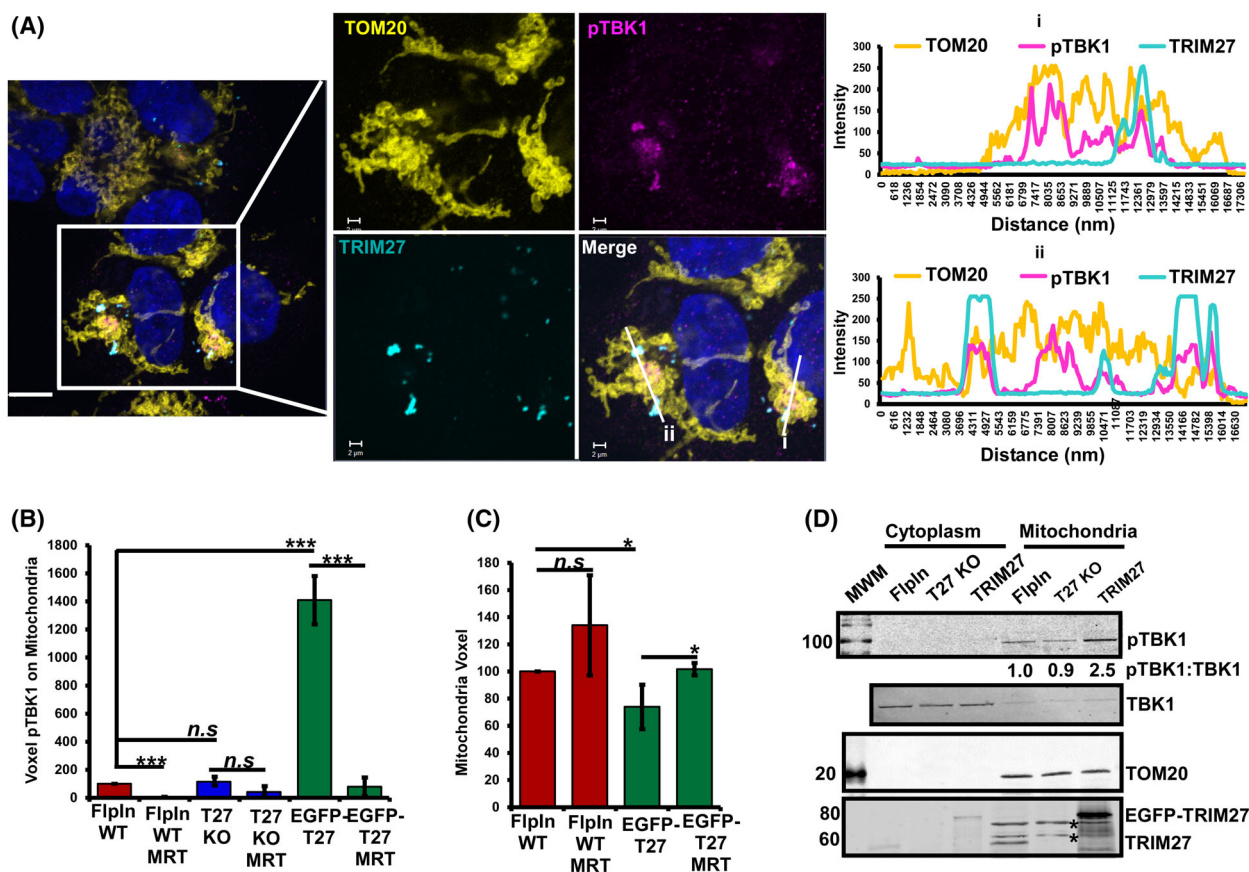
Fig. 7. pTBK1 is stabilized on the clustered mitochondria and implicated in the TRIM27-mediated mitochondria clustering. (A) Immunostaining of mitochondria (TOM20) and pTBK1 in HEK293 FlpIn TRIM27 KO reconstituted with inducible expression of EGFP-TRIM27. Images were obtained using a LSM780 confocal laser scanning microscope, and the co-localization line plots to the right obtained using the ZEN LITE software (ZEISS). Scale bar: 10 μm, on magnification 2 μm. (B) Quantification of the amount of pTBK1 localized on mitochondria in HEK293 FlpIn, HEK293 FlpIn TRIM27 KO and HEK293 FlpIn TRIM27 KO EGFP-TRIM27 cell lines under normal conditions, and upon treatment with the TBK1 inhibitor MRT67307 (MRT). Quantification of the pTBK1 voxel on mitochondria was performed using VOLOCITY software (Perkin Elmer). The graphs represent the average of three independent experiments with SD, each experiment including > 100 cells per condition. ***$P < 0.0005$, n.s.: not significant (Student's *t*-test). (C) Quantification of the amount of mitochondria (TOM20 intensity and volume) in HEK293 FlpIn and HEK293 FlpIn TRIM27 KO EGFP-TRIM27 cell lines under normal conditions and upon treatment with the TBK1 inhibitor MRT67307 (MRT). Quantification of mitochondria voxel was performed using VOLOCITY software (Perkin Elmer). The graphs represent the average of three independent experiments with SD, each experiment including > 100 cells per condition. *$P < 0.05$, n.s.: not significant (Student's *t*-test). (D) Western blot analysis of pTBK1, TBK1, and TRIM27 detected in the cytoplasmic and mitochondria extracts isolated from HEK293 FlpIn, HEK293 FlpIn TRIM27 KO cells reconstituted with EGFP-TRIM27 expression. Antibodies against TOM20 verify the enrichment of the mitochondrial fractions. * Indicates unspecific bands detected by the TRIM27 antibody.

reconstituted cells (Fig. 7B). Addition of the TBK1 inhibitor MRT67307 leads to a significant loss of pTBK1 on the mitochondria in the HEK293 FlpIn cells and the HEK293 FlpIn TRIM27 KO cells reconstituted with EGFP-TRIM27, but not in the HEK293 FlpIn TRIM27 KO cells (Fig. 7B). Moreover, inhibiting TBK1 reduced the clustering of mitochondria in the EGFP-TRIM27-expressing cells (Fig. 7C), indicating that the TRIM27-mediated mitochondria clustering acts via TBK1 activation. To further verify that pTBK1 is enriched on mitochondria in the HEK293

FlpIn TRIM27 KO EGFP-TRIM27 cells, mitochondria was isolated from the HEK293 FlpIn, HEK293 FlpIn TRIM27 KO and reconstituted cell lines, and the amount of pTBK1 in the mitochondrial fraction identified by western blotting (Fig. 7D). The blots show that pTBK1 is highly enriched in the mitochondria fractions, compared with unphosphorylated TBK1 which is mainly localized in the cytoplasm. TRIM27, both endogenous and the reconstituted EGFP-TRIM27, is enriched in the mitochondria fraction compared with the cytoplasmic fraction. Partial

co-localization of TRIM27 with the mitochondria has been reported previously [25]. Together these results show that pTBK1 is stabilized on the EGFP-TRIM27-mediated mitochondria clusters and that inhibiting TBK1 activity reduces the EGFP-TRIM27 induced mitochondria clustering. Hence, the TRIM27-mediated mitochondria clustering seems to be facilitated by active TBK1.

## TRIM27 facilitates mitophagy via TBK1

Cells lacking TBK1 are deficient in depolarization-dependent mitophagy, and several studies have implicated TBK1 as an important player both in PINK1/PARKIN-mediated mitophagy [33,34,56] and in PINK1/PARKIN-independent mitophagy [39]. TBK1 activation in response to mitochondrial depolarization promotes phosphorylation and efficient recruitment of SQSTM1/p62 to depolarized mitochondria [34]. TBK1 phosphorylation of SQSTM1/p62 at S403 leads to efficient binding of SQSTM1/p62 to ubiquitylated mitochondria [35,54]. Hence, our next question was if TRIM27 plays a role in mitophagy. Mitophagy is a rare happening in cells grown under normal condition. To be able to quantify mitophagy events in many cells, we induced mitophagy in the HEK293 FlpIn, HEK293 FlpIn TRIM27 KO and the HEK293 FlpIn TRIM27 KO reconstituted with expression of EGFP-TRIM27. Mitophagy induction was obtained by co-overexpression of FKBP8 and LC3A, and autophagic degradation of mitochondria was measured using the double-tag mCherry-EGFP-OMP25TM [57] (Fig. 8A). In the HEK293 FlpIn cells, co-overexpression of FKBP8 and LC3A induced mitophagy in 23 ($\pm$5)% of the cells (Fig. 8A). However, in the HEK293 FlpIn

TRIM27 KO cells, the amount of cells undergoing mitophagy by FKBP8 and LC3A overexpression was reduced to 14 ($\pm$2)% (Fig. 8A). Importantly, in the cells reconstituted with TRIM27 expression the mitophagy activity was increased substantially to 48 ($\pm$2)%. (Fig. 8A), and a large number of RedOnly mitochondria were observed in the vicinity of the mitochondria clusters. The indicative of promoted mitophagy activity in the TRIM27-mediated mitochondria clusters was further supported by association of the early autophagy protein ATG7, and the late autophagy proteins LC3B and LAMP1 with the clustered mitochondria (Fig. 8B). To pinpoint whether active TBK1 is implicated in the TRIM27-mediated mitophagy, the mitophagy assay was repeated with the TBK1 inhibitor MRT67307. Figure 8C displays that the TBK1 inhibitor significantly impairs mitophagy in the HEK293 FlpIn cells and the HEK293 FlpIn TRIM27 KO cells reconstituted with expression of TRIM27, but not in the HEK293 FlpIn TRIM27 KO cells. Together these results show that expression of TRIM27 facilitates mitophagy in a TBK1-dependent way.

Discussion

This study originated from a double-tag assay of various TRIM proteins, in order to identify TRIMs that were degraded by autophagy [13]. Our hypothesis was that TRIMs that are directed to degradation in the lysosome may have a role in regulation of the autophagy process. We observed that mCherry-EYFP-TRIM27 formed RedOnly puncta both in normal conditions and upon starvation. In this work, we show that degradation of TRIM27 can happen via

Fig. 8. TRIM27 facilitates mitophagy in a pTBK1-dependent way. (A) HEK293 FlpIn cells, HEK293 TRIM27 KO cells and HEK293 TRIM27 KO cells reconstituted with EGFP-TRIM27 were transiently transfected with expression plasmids for the mitochondria marker mCherry-EGFP-OMP25TM, 3xFlag LC3A and mitophagy receptor myc-FKBP8. The appearance of RedOnly structures indicates acidified mitochondria. The images were obtained using a LSM780 (ZEISS) fluorescent confocal microscope. The graphs to the right represent quantification of the cells displaying RedOnly dots indicative of mitophagy activity. The bars represent the average with s. (D). Of three independent experiments, each including > 100 cells per condition. *: $P < 0.05$; ***: $P < 0.0005$; n.s.: $P > 0.05$ (Student's t-test). Scale bar: 10 μm. (B) Confocal images of the HEK293 FlpIn TRIM27 KO cells with inducible expression of EGFP-TRIM27 (0.1 μg·μL^{-1} doxycycline, 20 h) fixed and stained with anti-ATG7, anti-LC3B or anti-LAMP1 antibodies, respectively. The images were obtained using a LSM880 confocal microscope with Airyscan module (ZEISS). Scale bars: 10 μm. (C) Quantification of cells containing RedOnly mitochondria in the HEK293 FlpIn, HEK293 FlpIn TRIM27 KO and HEK293 FlpIn TRIM27 KO reconstituted with inducible expression of EGFP-TRIM27 (0.1 μg·μL^{-1} doxycycline, 20 h). The cells were co-transfected with expression plasmids for myc-FKBP8, Flag-LC3A and the double-tag mitochondria marker mCherry-EGFP-OMP25TM, and the cells were grown in normal media or media containing the TBK1 inhibitor MRT67307 (MRT, 5 μM, 20 h). The graphs represent the average with SD of three independent experiments, each including > 40 cells per condition. *: $P < 0.05$; ***: $P < 0.0005$; n.s.: $P > 0.05$ (Student's t-test). (D) A model depicting the role of TRIM27 as a crowding platform for TBK1 by direct interactions, leading to TBK1 activation via trans-autophosphorylation. TRIM27 also interacts with SQSTM1/p62, while TBK1 can facilitate the binding of SQSTM1/p62 to ubiquitylated substrates by S403 phosphorylation. This complex is in this way a self-reinforcing structure that will facilitate mitochondria clustering and mitophagy.

(A) mCherry-EGFP-OMP25TM

(B) FlpIn TRIM27KO EGFP-TRIM27

(C)

(D)
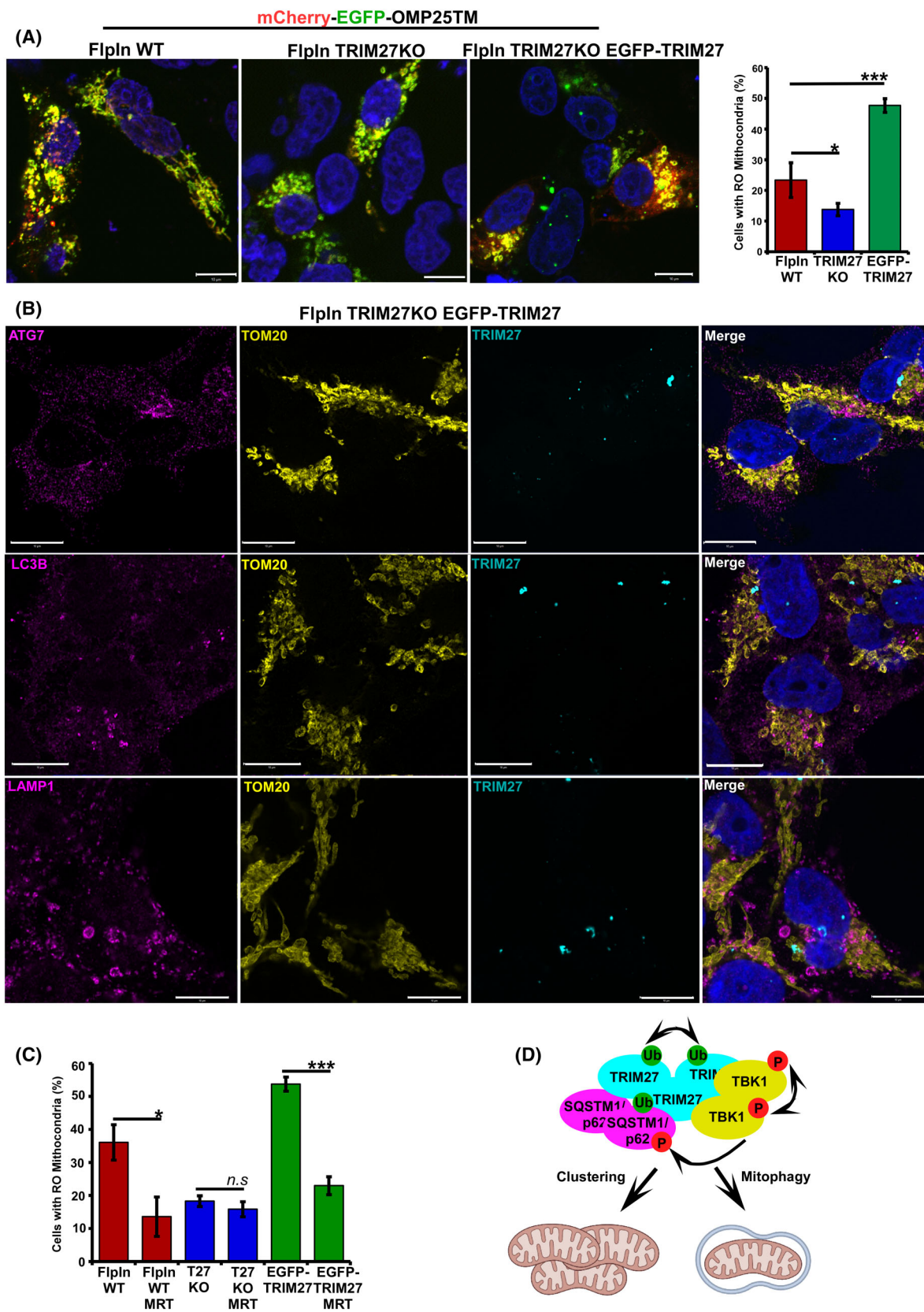
autophagy pathways and that the core autophagy proteins ATG7, ATG9 and the SQSTM1-like family of autophagy receptors are required for this degradation.

It is recently shown that the only transmembrane autophagy protein ATG9 plays an important role in the nucleation of the autophagosome [58]. ATG9 vesicles traffics from Golgi to endosomes in a ULK1-dependent manner under stress conditions [59], and ULK1 phosphorylation regulates trafficking of ATG9 under autophagy-inducing conditions [60]. In this work, we show that depletion of ATG9 leads to increased levels of TRIM27. TRIM27 seems to be modified in the ATG9 KO cells, resulting in a slower migrating band visualized by western blotting. In addition, the autophagy receptors SQSTM1/p62 and NBR1 displayed increased protein levels in the ATG9 KO cells and occurred as slower migration bands on the western blot membranes. This clearly points to TRIM27 as an autophagy substrate similar to NBR1 and SQSTM1/p62.

Furthermore, we identified SQSTM1/p62 as a mediator for autophagic degradation of TRIM27. In the reconstituted HEK293 FlpIn TRIM27KO cells, inducible expressed EGFP-TRIM27 forms cytoplasmic bodies of various sizes, in addition to some nuclear dots. This is similar to the localization pattern of endogenous TRIM27 in HEK293 cells reported by others [44]. TRIM family proteins, including TRIM27, dimerize through their coiled-coil region, and self-association seems to be a requirement for catalytic activity [61,62]. Moreover, it is proposed that substrate binding might induce higher-order oligomers that enhance their activity further [63]. Here, we show that the cytoplasmic EGFP-TRIM27 bodies are highly ubiquitylated and that SQSTM1/p62 associates with these bodies. However, the TRIM27 KO cells reconstituted with inducible expression of TRIM27 also contained SQSTM1/p62 aggregates that did not co-localize with TRIM27 bodies, indicating that TRIM27 can induce SQSTM1/p62 aggregation without being a scaffold itself. Importantly, many of these SQSTM1/p62 aggregates were localized on clustered mitochondria.

The Ser/Thr kinase TBK1, which originally was identified as a central regulator of innate immune responses, is now known to also be an important player in autophagy signalling pathways. TBK1 facilitates recruitment of the ULK complex to damaged mitochondria leading to mitophagy [37] and to cytosol-invading bacteria leading to xenophagy [64]. Recruitment of TBK1 to mitochondria induces TBK1 S172 autophosphorylation [37]. A direct interaction between TRIM27 and TBK1 has been described previously [19]. TRIM27 ubiquitylates TBK1 at lysine

residues K251 and K372, leading to its proteasomal degradation. The strong enrichment of phosphorylated TBK1 in cytoplasmic TRIM27 bodies observed in this study can be explained by their direct interaction. TBK1 is activated by trans-autophosphorylation on S172 when TBK1 dimers are brought together and oligomerize [65]. Hence, direct recruitment of TBK1 to TRIM27 bodies will lead to its oligomerization and activation by trans-autophosphorylation. Phosphorylated TBK1 was highly enriched on the clustered mitochondria and in the mitochondria fractions of the TRIM27 KO cells reconstituted with EGFP-TRIM27 compared with the HEK293 FlpIn cells and the TRIM27 KO cells. The amount of TBK1 was similar in TRIM27 KO cells and TRIM27 KO cells reconstituted with EGFP-TRIM27, and TBK1 was not enriched in the mitochondria fraction. Thus, in our HEK293 FlpIn cells, TRIM27 does not induce the degradation of TBK1. Instead, EGFP-TRIM27 mediates the stabilization of active TBK1 in TRIM27 bodies and on clustered mitochondria. Ablation of TRIM27 alleviates mitochondrial clustering and reduces mitophagy to a similar extent as in the TRIM27 KO cells and the HEK293 FlpIn cells that were treated with a TBK1 inhibitor. This suggests that the activation of TBK1 on the mitochondria is important for the TRIM27-mediated enhancement of mitophagy. Recently, it was shown that PARKIN associates with TBK1 and mediates ubiquitylation of TBK1 on the lysine residues K30 and K401 in cardiomyocytes [66]. These ubiquitylation events lead to the activation of TBK1, facilitating mitophagy via S403 phosphorylation of SQSTM1/p62. They propose an important role for the PARKIN-TBK1-SQSTM1/p62 axis in alleviating cardiac ageing and that its suppression will lead to mitochondrial dysfunction and apoptosis. Similarly, our results suggest that a TRIM27-TBK1-SQSTM1/p62 pathway exists in HEK293 cells and that this axis facilitates clustering and autophagic degradation of mitochondria (Fig. 8D).

TRIM27 is highly expressed in various cancers including breast, endometrial, ovarian, lung, colon and colorectal cancer, and colitis and colitis-associated carcinogenesis [17,21,46,67–71]. In this study, we connect TRIM27 to mitochondrial homeostasis, showing that it promotes mitophagy via TBK1 activation. Dysfunction of mitophagy is closely connected to tumorigenesis and tumour development [72]. In healthy cells, mitophagy maintains normal cell metabolism and inhibits tumorigenesis, while in cancer cells mitophagy improves the survival of tumour cells and supports the metastasis process [73,74]. One mechanism for the oncogenic potential of TRIM27 can be explained by

its ability to promote the degradation of dysfunctional mitochondria, supporting survival and metastasis of tumour cells.

Materials and methods

Antibodies and reagents

The following primary antibodies were used: rabbit polyclonal antibody for TRIM27 (Proteintech, Manchester, England, #122205-1-AP; 1 : 1000); rabbit polyclonal anti-GFP (Abcam, Cambridge, England, ab290; 1 : 5000); rabbit polyclonal anti-LC3B (Sigma, Darmstadt, Germany, L7543; 1 : 1000 for WB, 1 : 500 for IF); LAMP1 (Sigma, L1418, 1 : 200 for IF), ATG13 (Cell Signalling 13468S, 1 : 100 for IF), ULK1 (Cell Signalling 8054, 1 : 100 for IF), GM130 (Abcam Ab 53649, 1 : 500 for IF), USP7 (Biosite, Solihull, England, A300-033A, 1 : 200 for IF), NBR1 (Santa Cruz Sc-130380, 1 : 1000 for WB, 1 : 200 for IF), TOM20 (Santa Cruz Sc-11415, Dallas, TX, USA,1 : 500 for IF), FK2 (AH Diagnostics BML-PW8810-0100, Aarhus, Denmark, 1 : 1000 for WB, 1 : 500 for IF); mouse monoclonal anti-p62/SQSTM1 lck ligand (BD Biosciences, 610833; 1 : 2000) and guinea pig polyclonal anti-p62/SQSTM1 (Progen, Heidelberg, Germany, GP62/SQSTM1-C; 1 : 2000); WIPI2 (Abcam, ab105459, 1 : 500 for IF), ATG9a (Abcam, ab108338, 1 : 1000), NDP52 (Cell Signalling,#60732, 1 : 1000), TBK1 (Millipore, Burlington, MS, USA, #04-856, 1 : 500), pTBK1 (Cell Signalling, #5483, 1 : 1000 for WB, 1 : 200 for IF), calreticulin (Cell Signalling, #12238, 1 : 200 for IF), TIM23 (BD Biosciences, Heidelberg, Germany, #611223, 1 : 2000), mouse monoclonal anti-PCNA (DAKO, Santa Clara, CA, USA, M0879; 1 : 1000). The following secondary antibodies were used: Horseradish-peroxidase (HRP)-conjugated goat anti-rabbit IgG (BD Biosciences, 554021; 1 : 2000); HRP-conjugated goat anti-mouse Ig (BD Biosciences, 554002; 1 : 2000); and HRP-conjugated anti-Biotin antibody (Cell Signalling, #7075; 1 : 2000). The following fluorescent secondary antibodies were used: Alexa Fluor® 488-conjugated goat anti-mouse IgG (Life Technologies, Carlsbad, CA, USA, A-11029; 1 : 1000); Alexa Fluor® 555-conjugated goat anti-rabbit IgG (Life Technologies, A-11008; 1 : 5000); Alexa Fluor® 555-conjugated goat anti-mouse IgG (Life Technologies, A-21424; 1 : 1000); Alexa Fluor® 647-conjugated goat anti-guinea pig IgG (Life Technologies, A-21450; 1 : 1000). The reagents used were Bafilomycin A1 (Sigma, B1793); MG132 (Sigma, C2759); Tetracycline (Sigma, #87128); Hanks Balanced salt solution (Sigma, H8264), MRT67307 (Sigma, 1190378-57-4).

Construction of plasmids

All plasmids used in this study are listed in Table 1. Plasmids were made by use of the Gateway recombination

Table 1. Plasmids used in this study.

pDONR221 TRIM27	Harvard HsCD00042999
pDEST-mCherry-EYFP TRIM27	[13]
pDEST-EGFP-C1	[75]
pDEST-EGFP-TRIM27	This study
pDEST-Myc-TRIM27	This study
pDEST-Myc-SQSTM1/p62	[75]
pGEX-SQSTM1/p62	[75]
pDest-Myc-FKBP8	[57]
pDest-mCherry-EYFP-OMP25-TM	[57]
pDest-3XFlag-LC3A	[57]
pSPCas9(BB)-2A-GFP (PX458)	[43] Addgene#48138
pDEST-EGFP FlpIn TRIM27	This study

system (ThermoFisher, Carlsbad, CA, USA). Gateway LR reactions were performed as described in the instruction manual. All plasmids were verified by restriction enzyme digestion and DNA sequencing (BigDye, Applied Biosystems, Waltham, MA, USA, 4337455).

Cell culture and transfections

HeLa (ATCC, CCL2), Hek293 (ATCC, Manassas, VA, USA, CRL-1573) and Hek293 T-Rex (ThermoFisher, R714-07) cells were cultured in Dulbecco's modified eagle's medium (DMEM; Sigma, D6046) with 10% fetal bovine serum and 1% streptomycin–penicillin (Sigma, P4333). Hek FlpIn T-Rex cells with integrated EGFP-TRIM27, and the various HEK293 FlpIn KO cell lines, were grown in the same medium with additional selection marker antibiotics, 200 µg·mL^{-1} Hygromycin B (Invitrogen, Waltham, MA, USA, #10687010) and 7.5 µg·mL^{-1} Blasticidin (Gibco, Waltham, MA, USA, A1113903). Subconfluent cells were transfected using TransIT-LT1 (Mirus, Mirus, GE, USA, MIR2300) or Metafectene Pro (Biontex, München, Germany, T040) following the manufacturer's instructions. All cell lines were routinely tested for mycoplasma contamination.

Recombinant protein production and GST-pulldown analysis

GST or GST-tagged SQSTM1/p62 were expressed in *E. coli* strain SoluBL21 (Genlantis, San Diego, CA, USA, #C700200). Protein expression was induced by treating overnight bacterial culture with 50 µg·mL^{-1} Isopropyl β-D-1-thiogalactopyranoside (IPTG). GST or GST fusion proteins were purified and immobilized on Glutathione Sepharose 4 Fast Flow beads (GE Healthcare, Chicago, IL, USA, 17-5132-01). Myc-tagged TRIM27 were *in vitro* translated using the TNT T7 reticulocyte Lysate system (Promega, Madison, WI, USA, #14610) in the presence of ^{35}S-methionine. *In vitro* translated protein or total cell lysate was pre-incubated with 10 µL Glutathione Sepharose beads and 100 µL of NETN buffer (50 mM Tris pH 8.0; 150 mM

NaCl; 1 mM EDTA; 0.5% Nonidet P-40) with cOmplete Mini EDTA-free protease inhibitor mixture tablets (Roche Applied Science, Penzberg, Germany, 11836170001) for 1 h at 4 °C to reduce unspecific binding. Pre-incubated lysate was then incubated with the immobilized GST fusion protein for 2 h at 4 °C. Beads were washed five times with NETN buffer, boiled with 2×SDS gel loading buffer (125 mM Tris pH 7.5; 4% SDS; 0.04% bromophenol blue; 8% sucrose; 100 mM dithiothreitol) and subjected to SDS/PAGE. Gels were stained with Coomassie Brilliant Blue R-250 Dye (Thermofisher Scientific, #20278) to visualize GST fusion proteins and then vacuum-dried. Signals from ^{35}S-labelled proteins were detected by a Fujifilm bioimaging analyser BAS-5000 (Fujifilm, Tokyo, Japan).

Western blotting

Cells were seeded in 6-well dishes and treated as indicated. Cells were lysed in 1×SDS loading buffer (50 mM Tris pH 7.4; 2% SDS; 10% Glycerol) supplemented with 200 mM dithiothreitol (DTT, Sigma, #D0632) and heated at 100 °C for 10 min. Protein concentration was measured using the Pierce BCA Protein Assay Kit (Thermofisher Scientific, #23227). Equal amounts of protein were resolved by SDS/PAGE and transferred to nitrocellulose membrane (Sigma, GE10600003). The membrane was stained with Ponceau S (Sigma, P3504), blocked with 5% non-fat dry milk in 1% PBS-T (0.2 M Tris pH 8; 1.5 M NaCl and 0.05% Tween20 (Sigma, P9416)) for 1 h and then incubated with indicated primary antibodies for 24 h. The membrane was washed three times for 10 min each with PBS-T followed by incubation with secondary antibody for 1 h. The membrane was washed three times for 10 min and analysed by enhanced chemiluminescence using the IMAGEQUANT LAS 4000 (GE Lifescience, Chicago, IL, USA) or scanned on ODYSSEY CLX IMAGER (Li-Cor, Lincoln, NE, USA).

Immunostaining and fluorescence confocal microscopy

Subconfluent cells grown in 24-well plates on coverslips (VWR, Radnor, PA, USA, #631-0150) coated with Fibronectin (Sigma, F1141) or poly-L-Lysine (Sigma, P8920) were treated as indicated. They were fixed in 4% formaldehyde for 15 min. The cells were then permeabilized with 0.05% Saponin in PBS at RT for 5 min and incubated at room temperature 1 h with a specific primary antibody diluted in PBS with 0.05% Saponin, followed by incubation 1 h at RT with Alexa Fluor 488-, 555- or 647-conjugated secondary antibody diluted in PBS with 0.05% saponin and DAPI (Thermo Scientific, 1 : 5000). Confocal images were obtained using a 63×/NA1.4 oil immersion objective on an LSM780 (ZEISS) or LSM880 (ZEISS). Quantification of cells containing RedOnly dots in the double-tagged screen was done manually in three independent

experiments. Quantification of mitochondria voxel and pTBK1 voxel on mitochondria was performed on z-stack images of at least 100 cells per condition using VOLOCITY (Perkin Elmer, Waltham, MA, USA), in three independent experiments.

Generation of TRIM27 knockout in HEK293 FlpIn cell lines

To generate knockout cells for TRIM27, the CRISPR/Cas9 system was exploited as described by Ran et al. [43]. The Guide RNA sequence 5'-CTTTACCAGTTGGGTCACGT-3' was ligated into the vector pSpCas9(BB)-2A-GFP (PX458; Addgene, Waltham, MA, USA, #48138) using BbsI restriction sites. Subconfluent Hek293 FlpIn T-Rex cells were transfected with the targeting plasmid using Metafectene Pro (Biontex, T020). EGFP-positive cells were sorted by FACS and plated into 96-well plates 3-day post-transfection. Single colonies were expanded up to 12-well plates and KO validated by immunoblotting. Confirmed KO clones were further screened by genomic sequencing. The targeted genomic regions were amplified by PCR using the primers 5'-CCGGAGAGAGCGCCGGAGAGTTG-3' and 5'-CAAGGTGAGGGCGCGGATCCGGGAG-3' and the resulting PCR products ligated into the pGEM-T-EASy vector (Promega, A3600). Sequencing was conducted for at least 3 clones for each PCR product.

Generation of tetracycline-inducible HEK293 FlpIn cell lines

The stable HEK293 FlpIn TRIM27 KO EGFP-TRIM27 cell line was generated using the HEK293 FlpIn T-Rex system (Thermofisher, R71407). TRIM27 cDNA was transferred to the inducible FlpIn expression vector pDEST-EGFP FlpIn by GATEWAY cloning. HEK293 FlpIn T-Rex TRIM27 KO cells were then co-transfected with the TRIM27 FlpIn expression vector and the FlpIn recombinase vector pOG44 in the ratio of 1 : 3. Cells were selected by treatment with 200 µg·mL^{-1} Hygromycin B (Invitrogen, #10687010) and 7.5 µg·ml^{-1} Blasticidin (Gibco, #A1113903), and protein expression verified by induction with Tetracycline (Sigma, #87128) or Doxycycline (Sigma, #D3447).

Cell proliferation assay

The cell lines HEK293 T-REx FlpIn, HEK293 T-Rex FlpIn TRIM27 KO, HEK293 T-REx FlpIn TRIM27 KO EGFP-TRIM27 and HEK293 T-REx FlpIn TRIM27 KO EGFP were harvested with trypsin and seeded into 12-well plates at a density of 10^5 cells per well. Afterwards, cells were incubated in IncuCyte (Essen BioScience, Ann Arbor, MI, USA) at 10× magnification and images were taken in the phase and green channels every 24 h. Images were analysed

by Incucyte S3 Live-cell analysis system. The assays were performed in triplicate.

Migration assay

The cell lines HEK293 T-REx FlpIn, HEK293 T-REx FlpIn TRIM27 KO, HEK293 T-REx FlpIn TRIM27 KO EGFP-TRIM27 and HEK293 T-REx FlpIn TRIM27 KO EGFP were harvested with trypsin and seeded into 96-well Image-Lock Microplate (Essen BioSystems) at a density of 8000 cells per well. Twenty-four hours after seeding, a scratch wound was made by using the Incucyte 96-well WoundMaker tool (Essen BioScience) according to the manufacturer's instructions. Cells were incubated at 37 °C with CO_2 in the Incucyte (Essen BioScience) at $10\times$ magnification, and pictures were taken in the phase and green channels every 15 h (for figure presentation, quantification every 24 h is shown). Images were analysed by Incucyte S3 Live-cell analysis system. The assay was repeated independently two times.

Mitochondria isolation assay

Subcellular fractionation was performed with a QProteome Mitochondria Isolation kit (Qiagen) according to the instruction manual. All steps were performed at 4 °C. In brief, $\leq 1 \times 10^7$ HEK293 FlpIn T-REx cells, TRIM27 KO cells and TRIM27 KO cells reconstituted with EGFP-TRIM27 were resuspended in 1 mL of lysis buffer (supplemented with $1\times$ Protease inhibitor), incubated for 10 min at 4 °C in an end-over-end shaker and centrifuged at $1000 \times g$ for 10 min. The supernatant which contains the cytosolic fractions was transferred into separate tubes, while the pellet was resuspended in 1.5 mL of ice-cold disruption buffer (supplemented with $1\times$ Protease inhibitor), rapidly passed through 21 g needle 10 times to disrupt cells and centrifuged at $1000 \times g$ for 10 min. The pellet was saved as nuclear fraction, while the supernatant was re-centrifuged at $6000 \times g$ for 10 min, 4 °C. The pellet obtained after centrifugation comprised the mitochondrial fraction, while the supernatant contained the microsomal fraction. The steps for high-purity preparations were followed according to the instruction manual. The pellet was resuspended in 750 µL Mitochondria Purification Buffer. A 2 mL tube was prepared with 750 µL Mitochondria Purification Buffer, 500 µL Disruption buffer (with Protease inhibitor) pipetted in the bottom, and the resuspended pellet was pipetted on top of the Mitochondria Purification Buffer. The tubes were centrifuged at $14\,000 \times g$ for 15 min, 1.5 mL of the supernatant was removed, and the last 0.5 mL which contains the mitochondria was transferred to a new tube. The mitochondrial fraction was diluted with 1.5 mL Mitochondria Storage Buffer and centrifuged at $8000 \times g$ for 10 min. Removed 1.5 mL, diluted again and centrifuged again at the same speed. This was

repeated until a pellet was formed. The pellet at last was resuspended in 100 µL Mitochondria Storage Buffer and stored at −70 °C.

Mitophagy assay

HEK293 FlpIn T-Rex cells, TRIM27 KO cells and TRIM27 KO cells reconstituted with EGFP-TRIM27 were seeded on poly-L-lysine-coated (SIGMA) coverslips 2 days before transient co-transfection with the plasmids mCherry-EYFP-OMP25-TM (100 ng), pDEST-3xFlag-LC3A (100 ng) and pDEST-myc-FKBP8 (100 ng) using the TransIT (Mirus) transfection reagent. One-day post-transfection, the cells were fixated in 4% Formaldehyde, 15 min at R.T., stained with DAPI (5 min). The cells were imaged using a Zeiss780 confocal microscope, and z-stack images of at least 100 cells per condition per experiment were manually quantified for RedOnly structures using the ZEN software (ZEISS, Oberkochen, Germany).

Correlative light and electron microscopy (CLEM)

Cells were seeded on glass-bottom dishes (Mattek cat. no. P35G-1.5-14-CGRD) with an engraved grid pattern to permit the correlation of dish coordinates between light microscope images and the resin block face prior to ultramicrotomy. HEK293 FlpIn TRIM27 KO EGFP-TRIM27 cells were treated with doxycycline (0.1 µg·mL^{-1}) for inducible expression of EGFP-TRIM27 1 day after seeding. The day after, cells were stained for DAPI and fixed in pre-warmed (37°°C) fixative containing 4% formaldehyde and 0.5% glutaraldehyde in PHEM buffer (60 mM PIPES, 25 mM HEPES, 10 mM EGTA, 4 mM $MgSO_4 \cdot 7H_2O$). Cells were then imaged by confocal microscopy with a $40\times$/NA1.2 water immersion objective. After confocal microscopy, cells were microwave-processed using additional fixatives and contrast agents for electron microscopy: 0.05% Malachite green/0.5% glutaraldehyde/0.1% PHEM Buffer, 1% osmium tetroxide/0.8% $K_3Fe(CN)_6$ in PHEM buffer, 1% tannic acid in ddH_2O and 1% uranyl acetate in ddH_2O. Finally, samples went through stepwise ethanol dehydration (30% – 60% – 96% – 100%) and embedding in EPON resin. The resin was polymerized at 60°°C for 48 h and then trimmed to the relevant dish coordinate. Seventy nanometre sections were cut using a diamond knife (Diatome) on a ultramicrotome RMC Atumtome and picked up on formvar-coated mesh grids. Sections were imaged using a Hitachi HT7800 120 kV Transmission Electron Microscope. Correlation was performed using MIRRORCLEM software (Hitachi, Stoke Poges, England).

Statistics

All experiments were repeated at least three times, unless otherwise specified. Error bars represent standard

deviations (SD). Two-sided unpaired homoscedastic Student's *t*-tests were performed to assess significant differences between populations. Replicates were not pooled for statistical analyses.

Acknowledgements

Conflict of interest

The authors declare no conflict of interest.

Author contributions

ES conceptualized and designed the study. JGG, AKB, KSO, HCKBL, ZB, AB YPA and ES acquired the data. JGG, AKB, KSO and ES analysed the data. JGG, AKB and ES interpreted the data. JGG and ES wrote the original draft. ES, TL and TJ supervised the study.

Peer review

The peer review history for this article is available at https://publons.com/publon/10.1111/febs.16628.

Data availability statement

The data that support the findings of this study are available on request from the corresponding author.

References

1 Swatek KN, Komander D. Ubiquitin modifications. *Cell Res*. 2016;**26**:399–422.

2 Dikic I. Proteasomal and autophagic degradation systems. *Annu Rev Biochem*. 2017;**86**:193–224.

3 Kwon YT, Ciechanover A. The ubiquitin code in the ubiquitin-proteasome system and autophagy. *Trends Biochem Sci*. 2017;**42**:873–86.

4 Watanabe M, Hatakeyama S. TRIM proteins and diseases. *J Biochem*. 2017;**161**:135–44.

5 Esposito D, Koliopoulos MG, Rittinger K. Structural determinants of TRIM protein function. *Biochem Soc Trans*. 2017;**45**:183–91.

6 Di Rienzo M, Romagnoli A, Antonioli M, Piacentini M, Fimia GM. TRIM proteins in autophagy: selective sensors in cell damage and innate immune responses. *Cell Death Differ*. 2020;**27**:887–902.

7 Mandell MA, Jain A, Arko-Mensah J, Chauhan S, Kimura T, Dinkins C, et al. TRIM proteins regulate autophagy and can target autophagic substrates by direct recognition. *Dev Cell*. 2014;**30**:394–409.

8 Di Rienzo M, Antonioli M, Fusco C, Liu Y, Mari M, Orhon I, et al. Autophagy induction in atrophic muscle cells requires ULK1 activation by TRIM32 through unanchored K63-linked polyubiquitin chains. *Sci Adv*. 2019;**5**:eaau8857.

9 Fusco C, Mandriani B, Di Rienzo M, Micale L, Malerba N, Cocciadiferro D, et al. TRIM50 regulates Beclin 1 proautophagic activity. *Biochim Biophys Acta Mol Cell Res*. 2018;**1865**:908–19.

10 Mandell MA, Jain A, Kumar S, Castleman MJ, Anwar T, Eskelinen EL, et al. TRIM17 contributes to autophagy of midbodies while actively sparing other targets from degradation. *J Cell Sci*. 2016;**129**:3562–73.

11 Kimura T, Jain A, Choi SW, Mandell MA, Schroder K, Johansen T, et al. TRIM-mediated precision autophagy targets cytoplasmic regulators of innate immunity. *J Cell Biol*. 2015;**210**:973–89.

12 Sparrer KMJ, Gableske S, Zurenski MA, Parker ZM, Full F, Baumgart GJ, et al. TRIM23 mediates virus-induced autophagy via activation of TBK1. *Nat Microbiol*. 2017;**2**:1543–57.

13 Overa KS, Garcia-Garcia J, Bhujabal Z, Jain A, Overvatn A, Larsen KB, et al. TRIM32, but not its muscular dystrophy-associated mutant, positively regulates and is targeted to autophagic degradation by p62/SQSTM1. *J Cell Sci*. 2019;**132**:jcs236596.

14 Tomar D, Singh R, Singh AK, Pandya CD, Singh R. TRIM13 regulates ER stress induced autophagy and clonogenic ability of the cells. *Biochim Biophys Acta*. 2012;**1823**:316–26.

15 Cao T, Borden KL, Freemont PS, Etkin LD. Involvement of the rfp tripartite motif in protein-protein interactions and subcellular distribution. *J Cell Sci*. 1997;**110**(Pt 14):1563–71.

16 Tezel G, Nagasaka T, Iwahashi N, Asai N, Iwashita T, Sakata K, et al. Different nuclear/cytoplasmic distributions of RET finger protein in different cell types. *Pathol Int*. 1999;**49**:881–6.

17 Ma Y, Wei Z, Bast RC Jr, Wang Z, Li Y, Gao M, et al. Downregulation of TRIM27 expression inhibits the proliferation of ovarian cancer cells in vitro and in vivo. *Lab Invest*. 2016;**96**:37–48.

18 Zaman MM, Shinagawa T, Ishii S. Trim27-deficient mice are susceptible to streptozotocin-induced diabetes. *FEBS Open Bio*. 2013;**4**:60–4.

19 Zheng Q, Hou J, Zhou Y, Yang Y, Xie B, Cao X. Siglec1 suppresses antiviral innate immune response by

inducing TBK1 degradation via the ubiquitin ligase TRIM27. *Cell Res.* 2015;25:1121–36.

20 Zhuang XJ, Tang WH, Feng X, Liu CY, Zhu JL, Yan J, et al. Trim27 interacts with Slx2, is associated with meiotic processes during spermatogenesis. *Cell Cycle.* 2016;15:2576–84.

21 Zoumpoulidou G, Broceno C, Li H, Bird D, Thomas G, Mittnacht S. Role of the tripartite motif protein 27 in cancer development. *J Natl Cancer Inst.* 2012;104:941–52.

22 Wang J, Teng JL, Zhao D, Ge P, Li B, Woo PC, et al. The ubiquitin ligase TRIM27 functions as a host restriction factor antagonized by mycobacterium tuberculosis PtpA during mycobacterial infection. *Sci Rep.* 2016;6:34827.

23 Conwell SE, White AE, Harper JW, Knipe DM. Identification of TRIM27 as a novel degradation target of herpes simplex virus 1 ICP0. *J Virol.* 2015;89:220–9.

24 Cai J, Chen HY, Peng SJ, Meng JL, Wang Y, Zhou Y, et al. USP7-TRIM27 axis negatively modulates antiviral type I IFN signaling. *FASEB J.* 2018;32(10):5238–49.

25 Zaman MM, Nomura T, Takagi T, Okamura T, Jin W, Shinagawa T, et al. Ubiquitination-deubiquitination by the TRIM27-USP7 complex regulates tumor necrosis factor alpha-induced apoptosis. *Mol Cell Biol.* 2013;33:4971–84.

26 Hao YH, Fountain MD Jr, Fon Tacer K, Xia F, Bi W, Kang SH, et al. USP7 acts as a molecular rheostat to promote WASH-dependent endosomal protein recycling and is mutated in a human neurodevelopmental disorder. *Mol Cell.* 2015;59:956–69.

27 Iorio R, Celenza G, Petricca S. Mitophagy: molecular mechanisms, new concepts on parkin activation and the emerging role of AMPK/ULK1 Axis. *Cell.* 2021;11:30.

28 Yamano K, Kikuchi R, Kojima W, Hayashida R, Koyano F, Kawawaki J, et al. Critical role of mitochondrial ubiquitination and the OPTN-ATG9A axis in mitophagy. *J Cell Biol.* 2020;219:e201912144.

29 Kane LA, Lazarou M, Fogel AI, Li Y, Yamano K, Sarraf SA, et al. PINK1 phosphorylates ubiquitin to activate parkin E3 ubiquitin ligase activity. *J Cell Biol.* 2014;205:143–53.

30 Kazlauskaite A, Kondapalli C, Gourlay R, Campbell DG, Ritorto MS, Hofmann K, et al. Parkin is activated by PINK1-dependent phosphorylation of ubiquitin at Ser65. *Biochem J.* 2014;460:127–39.

31 Koyano F, Okatsu K, Kosako H, Tamura Y, Go E, Kimura M, et al. Ubiquitin is phosphorylated by PINK1 to activate parkin. *Nature.* 2014;510:162–6.

32 Narendra DP, Jin SM, Tanaka A, Suen DF, Gautier CA, Shen J, et al. PINK1 is selectively stabilized on impaired mitochondria to activate parkin. *PLoS Biol.* 2010;8:e1000298.

33 Lazarou M, Sliter DA, Kane LA, Sarraf SA, Wang C, Burman JL, et al. The ubiquitin kinase PINK1 recruits autophagy receptors to induce mitophagy. *Nature.* 2015;524:309–14.

34 Heo JM, Ordureau A, Paulo JA, Rinehart J, Harper JW. The PINK1-PARKIN mitochondrial ubiquitylation pathway drives a program of OPTN/NDP52 recruitment and TBK1 activation to promote mitophagy. *Mol Cell.* 2015;60:7–20.

35 Matsumoto G, Shimogori T, Hattori N, Nukina N. TBK1 controls autophagosomal engulfment of polyubiquitinated mitochondria through p62/SQSTM1 phosphorylation. *Hum Mol Genet.* 2015;24:4429–42.

36 Richter B, Sliter DA, Herhaus L, Stolz A, Wang C, Beli P, et al. Phosphorylation of OPTN by TBK1 enhances its binding to Ub chains and promotes selective autophagy of damaged mitochondria. *Proc Natl Acad Sci USA.* 2016;113:4039–44.

37 Vargas JNS, Wang C, Bunker E, Hao L, Maric D, Schiavo G, et al. Spatiotemporal control of ULK1 activation by NDP52 and TBK1 during selective autophagy. *Mol Cell.* 2019;74:347–362 e6.

38 Onishi M, Yamano K, Sato M, Matsuda N, Okamoto K. Molecular mechanisms and physiological functions of mitophagy. *EMBO J.* 2021;40:e104705.

39 Seabright AP, Fine NHF, Barlow JP, Lord SO, Musa I, Gray A, et al. AMPK activation induces mitophagy and promotes mitochondrial fission while activating TBK1 in a PINK1-parkin independent manner. *FASEB J.* 2020;34:6284–301.

40 Nishida Y, Arakawa S, Fujitani K, Yamaguchi H, Mizuta T, Kanaseki T, et al. Discovery of Atg5/Atg7-independent alternative macroautophagy. *Nature.* 2009;461:654–8.

41 Ohsumi Y. Historical landmarks of autophagy research. *Cell Res.* 2014;24:9–23.

42 Orsi A, Razi M, Dooley HC, Robinson D, Weston AE, Collinson LM, et al. Dynamic and transient interactions of Atg9 with autophagosomes, but not membrane integration, are required for autophagy. *Mol Biol Cell.* 2012;23:1860–73.

43 Ran FA, Hsu PD, Wright J, Agarwala V, Scott DA, Zhang F. Genome engineering using the CRISPR-Cas9 system. *Nat Protoc.* 2013;8:2281–308.

44 Zurek B, Schoultz I, Neerincx A, Napolitano LM, Birkner K, Bennek E, et al. TRIM27 negatively regulates NOD2 by ubiquitination and proteasomal degradation. *PLoS ONE.* 2012;7:e41255.

45 Harbers M, Nomura T, Ohno S, Ishii S. Intracellular localization of the ret finger protein depends on a functional nuclear export signal and protein kinase C activation. *J Biol Chem.* 2001;276:48596–607.

46 Zhang Y, Feng Y, Ji D, Wang Q, Qian W, Wang S, et al. TRIM27 functions as an oncogene by activating epithelial-mesenchymal transition and p-AKT in colorectal cancer. *Int J Oncol.* 2018;53:620–32.

47 Geisler S, Holmstrom KM, Skujat D, Fiesel FC, Rothfuss OC, Kahle PJ, et al. PINK1/parkin-mediated mitophagy is dependent on VDAC1 and p62/SQSTM1. *Nat Cell Biol.* 2010;**12**:119–31.

48 Okatsu K, Saisho K, Shimanuki M, Nakada K, Shitara H, Sou YS, et al. p62/SQSTM1 cooperates with parkin for perinuclear clustering of depolarized mitochondria. *Genes Cells.* 2010;**15**:887–900.

49 Zhong Z, Sanchez-Lopez E, Karin M. Autophagy, NLRP3 inflammasome and auto-inflammatory/immune diseases. *Clin Exp Rheumatol.* 2016;**34**: 12–6.

50 Nguyen TD, Shaid S, Vakhrusheva O, Koschade SE, Klann K, Tholken M, et al. Loss of the selective autophagy receptor p62 impairs murine myeloid leukemia progression and mitophagy. *Blood.* 2019;**133**:168–79.

51 Moore AS, Holzbaur EL. Dynamic recruitment and activation of ALS-associated TBK1 with its target optineurin are required for efficient mitophagy. *Proc Natl Acad Sci USA.* 2016;**113**:E3349–58.

52 Zachari M, Gudmundsson SR, Li Z, Manifava M, Cugliandolo F, Shah R, et al. Selective autophagy of mitochondria on a ubiquitin-endoplasmic-reticulum platform. *Dev Cell.* 2019;**50**:627–643 e5.

53 Matsumoto G, Wada K, Okuno M, Kurosawa M, Nukina N. Serine 403 phosphorylation of p62/SQSTM1 regulates selective autophagic clearance of ubiquitinated proteins. *Mol Cell.* 2011;**44**:279–89.

54 Pilli M, Arko-Mensah J, Ponpuak M, Roberts E, Master S, Mandell MA, et al. TBK-1 promotes autophagy-mediated antimicrobial defense by controlling autophagosome maturation. *Immunity.* 2012;**37**:223–34.

55 Shu C, Sankaran B, Chaton CT, Herr AB, Mishra A, Peng J, et al. Structural insights into the functions of TBK1 in innate antimicrobial immunity. *Structure.* 2013;**21**:1137–48.

56 Heo JM, Ordureau A, Swarup S, Paulo JA, Shen K, Sabatini DM, et al. RAB7A phosphorylation by TBK1 promotes mitophagy via the PINK-PARKIN pathway. *Sci Adv.* 2018;**4**:eaav0443.

57 Bhujabal Z, Birgisdottir AB, Sjottem E, Brenne HB, Overvatn A, Habisov S, et al. FKBP8 recruits LC3A to mediate parkin-independent mitophagy. *EMBO Rep.* 2017;**18**:947–61.

58 Sawa-Makarska J, Baumann V, Coudevylle N, von Bulow S, Nogellova V, Abert C, et al. Reconstitution of autophagosome nucleation defines Atg9 vesicles as seeds for membrane formation. *Science.* 2020;**369**: eaaz7714.

59 Young AR, Chan EY, Hu XW, Kochl R, Crawshaw SG, High S, et al. Starvation and ULK1-dependent cycling of mammalian Atg9 between the TGN and endosomes. *J Cell Sci.* 2006;**119**:3888–900.

60 Zhou C, Ma K, Gao R, Mu C, Chen L, Liu Q, et al. Regulation of mATG9 trafficking by Src- and ULK1-mediated phosphorylation in basal and starvation-induced autophagy. *Cell Res.* 2017;**27**:184–201.

61 Koliopoulos MG, Esposito D, Christodoulou E, Taylor IA, Rittinger K. Functional role of TRIM E3 ligase oligomerization and regulation of catalytic activity. *EMBO J.* 2016;**35**:1204–18.

62 Streich FC Jr, Ronchi VP, Connick JP, Haas AL. Tripartite motif ligases catalyze polyubiquitin chain formation through a cooperative allosteric mechanism. *J Biol Chem.* 2013;**288**:8209–21.

63 Yudina Z, Roa A, Johnson R, Biris N, de Souza Aranha Vieira DA, Tsiperson V, et al. RING dimerization links higher-order assembly of TRIM5alpha to synthesis of K63-linked polyubiquitin. *Cell Rep.* 2015;**12**:788–97.

64 Ravenhill BJ, Boyle KB, von Muhlinen N, Ellison CJ, Masson GR, Otten EG, et al. The cargo receptor NDP52 initiates selective autophagy by recruiting the ULK complex to cytosol-invading bacteria. *Mol Cell.* 2019;**74**:320–329 e6.

65 Larabi A, Devos JM, Ng SL, Nanao MH, Round A, Maniatis T, et al. Crystal structure and mechanism of activation of TANK-binding kinase 1. *Cell Rep.* 2013;**3**:734–46.

66 Gao B, Yu W, Lv P, Liang X, Sun S, Zhang Y. Parkin overexpression alleviates cardiac aging through facilitating K63-polyubiquitination of TBK1 to facilitate mitophagy. *Biochim Biophys Acta Mol Basis Dis.* 2021;**1867**:165997.

67 Horio M, Kato T, Mii S, Enomoto A, Asai M, Asai N, et al. Expression of RET finger protein predicts chemoresistance in epithelial ovarian cancer. *Cancer Med.* 2012;**1**:218–29.

68 Iwakoshi A, Murakumo Y, Kato T, Kitamura A, Mii S, Saito S, et al. RET finger protein expression is associated with prognosis in lung cancer with epidermal growth factor receptor mutations. *Pathol Int.* 2012;**62**:324–30.

69 Jiang J, Xie C, Liu Y, Shi Q, Chen Y. Up-regulation of miR-383-5p suppresses proliferation and enhances chemosensitivity in ovarian cancer cells by targeting TRIM27. *Biomed Pharmacother.* 2019;**109**:595–601.

70 Tezel GG, Uner A, Yildiz I, Guler G, Takahashi M. RET finger protein expression in invasive breast carcinoma: relationship between RFP and ErbB2 expression. *Pathol Res Pract.* 2009;**205**:403–8.

71 Tsukamoto H, Kato T, Enomoto A, Nakamura N, Shimono Y, Jijiwa M, et al. Expression of ret finger protein correlates with outcomes in endometrial cancer. *Cancer Sci.* 2009;**100**:1895–901.

72 Chang JY, Yi HS, Kim HW, Shong M. Dysregulation of mitophagy in carcinogenesis and tumor progression. *Biochim Biophys Acta Bioenerg.* 2017;**1858**:633–40.

73 Vara-Perez M, Felipe-Abrio B, Agostinis P. Mitophagy in cancer: A tale of adaptation. *Cell*. 2019;**8**:493.

74 Wang Y, Liu HH, Cao YT, Zhang LL, Huang F, Yi C. The role of mitochondrial dynamics and mitophagy in carcinogenesis, metastasis and therapy. *Front Cell Dev Biol*. 2020;**8**:413.

75 Lamark T, Perander M, Outzen H, Kristiansen K, Overvatn A, Michaelsen E, et al. Interaction codes within the family of mammalian Phox and Bem1p domain-containing proteins. *J Biol Chem*. 2003;**278**:34568–81.